ILLINOIS STATE WATER SURVEY
Meteorology Laboratory
at the
University of Illinois
Urbana, Illinois

RAINDROP   SIZE   DISTRIBUTIONS   WITH
RAINFALL TYPES AND WEATHER CONDITIONS

by

Miyuki Fujiwara

RESEARCH REPORT NO. 8
sponsored by

U. S. Army signal Research and Development Laboratory
Fort Monmouth, New Jersey

1961

DATE DUE			

AD_____ Accession No._____
Illinois State Water Survey Division, Urbana,
Illinois. RAINDROP SIZE DISTRIBUTIONS WITH
RAINFALL TYPES AND WEATHER CONDITIONS - Miyuki
Fujiwara

Research Report No. 8, 1961, 48 pps. 15 figs.
(Contract DA-36-039 SC-87280) DA Task
3A99-07-001-01, Unclassified Report

This paper investigates the relationship be-
tween the variability of the raindrop size
distributions and weather conditions on the
basis of raindrop, radar, and synoptic
weather data. The first section reviews the
variability of the observed Z-R values in
relation to rainfall types; the second inter-
prets the behavior of Z-R points in terms of
N_D-D relationships proposed by the author; the
last discusses the relationships between the
parameters of the fitting equations and some
weather conditions.

UNCLASSIFIED

1. Radar Meteorology

2. Drop Size Distribution

3. Coalescence Theory

4. Cloud Physics

5. Contract DA-36-039 SC-87280

AD_____ Accession No._____
Illinois State Water Survey Division, Urbana,
Illinois. RAINDROP SIZE DISTRIBUTIONS WITH
RAINFALL TYPES AND WEATHER CONDITIONS - Miyuki
Fujiwara

Research Report No. 8, 1961, 48 pps. 15 figs.
(Contract DA-36-039 SC-87280) DA Task
3A99-07-001-01, Unclassified Report

This paper investigates the relationship be-
tween the variability of the raindrop size
distributions and weather conditions on the
basis of raindrop, radar, and synoptic
weather data. The first section reviews the
variability of the observed Z-R values in
relation to rainfall types; the second inter-
prets the behavior of Z-R points in terms of
N_D-D relationships proposed by the author; the
last discusses the relationships between the
parameters of the fitting equations and some
weather conditions.

UNCLASSIFIED

1. Radar Meteorology

2. Drop Size Distribution

3. Coalescence Theory

4. Cloud Physics

5. Contract DA-36-039 SC-87280

AD_____ Accession No._____
Illinois State Water Survey Division, Urbana,
Illinois. RAINDROP SIZE DISTRIBUTIONS WITH
RAINFALL TYPES AND WEATHER CONDITIONS - Miyuki
Fujiwara

Research Report No. 8, 1961, 48 pps. 15 figs.
(Contract DA-36-039 SC-87280) DA Task
3A99-07-001-01, Unclassified Report

This paper investigates the relationship be-
tween the variability of the raindrop size
distributions and weather conditions on the
basis of raindrop, radar, and synoptic
weather data. The first section reviews the
variability of the observed Z-R values in
relation to rainfall types; the second inter-
prets the behavior of Z-R points in terms of
N_D-D relationships proposed by the author; the
last discusses the relationships between the
parameters of the fitting equations and some
weather conditions.

UNCLASSIFIED

1. Radar Meteorology

2. Drop Size Distribution

3. Coalescence Theory

4. Cloud Physics

5. Contract DA-36-039 SC-87280

AD_____ Accession No._____
Illinois State Water Survey Division, Urbana,
Illinois. RAINDROP SIZE DISTRIBUTIONS WITH
RAINFALL TYPES AND WEATHER CONDITIONS - Miyuki
Fujiwara

Research Report No. 8, 1961, 48 pps. 15 figs.
(Contract DA-36-039 SC-87280) DA Task
3A99-07-001-01,

This paper investigates the relationship be-
tween the variability of the raindrop size
distributions and weather conditions on the
basis of raindrop, radar, and synoptic
weather data. The first section reviews the
variability of the observed Z-R values in
relation to rainfall types; the second inter-
prets the behavior of Z-R points in terms of
N_D-D relationships proposed by the author; the
last discusses the relationships between the
parameters of the fitting equations and some
weather conditions.

UNCLASSIFIED

1. Radar Meteorology

2. Drop Size Distribution

3. Coalescence Theory

4. Cloud Physics

5. Contract DA-36-039 SC-87280

AD   Accession No.
Illinois State Water Survey Division, Urbana,
Illinois., RAINDROP SIZE DISTRIBUTIONS WITH
RAINFALL TYPES AND WEATHER CONDITIONS - Miyuki
Fujiwara

Research Report No. 8, 1961, 48 pps. 15 figs.
(Contract DA-36-039 SC-87280) DA Task
3A99-07-001-01, Unclassified Report

This paper investigates the relationship be-
tween the variability of the raindrop size
distributions and weather conditions on the
basis of raindrop, radar, and synoptic
weather data. The first section reviews the
variability of the observed Z-R values in
relation to rainfall types; the second inter-
prets the behavior of Z-R points in terms of
N_D-D relationships proposed by the author; the
last discusses the relationships between the
parameters of the fitting equations and some
weather conditions.

UNCLASSIFIED

1. Radar Meteorology

2. Drop Size Distribution

3. Coalescence Theory

4. Cloud Physics

5. Contract DA-36-039 SC-87280

AD   Accession No.
Illinois State Water Survey Division, Urbana,
Illinois. RAINDROP SIZE DISTRIBUTIONS WITH
RAINFALL TYPES AND WEATHER CONDITIONS - Miyuki
Fujiwara

Research Report No. 8, 1961, 48 pps. 15 figs.
(Contract DA-36-039 SC-87280) DA Task
3A99-07-001-01, Unclassified Report

This paper investigates the relationship be-
tween the variability of the raindrop size
distributions and weather conditions on the
basis of raindrop, radar, and synoptic
weather data. The first section reviews the
variability of the observed Z-R values in
relation to rainfall types; the second inter-
prets the behavior of Z-R points in terms of
N_D-D relationships proposed by the author; the
last discusses the relationships between the
parameters of the fitting equations and some
weather conditions.

UNCLASSIFIED

1. Radar Meteorology

2. Drop Size Distribution

3. Coalescence Theory

4. Cloud Physics

5. Contract DA-36-039 SC-87280

Illinois State Water Survey-
Meteorology Laboratory
at the
University of Illinois
Urbana, Illinois

RAINDROP SIZE DISTRIBUTIONS WITH
RAINFALL TYPES AND WEATHER CONDITIONS

by

Miyuki Pujiwara

RESEARCH REPORT NO. 8

sponsored by

U. S. Army Signal Research and Development Laboratory
Port Monmouth, New Jersey

TABLE OP CONTENTS

TABLE OF CONTENTS (Cont'd)

ABSTRACT

This paper investigates the relationship between the variability of the raindrop size distributions and weather conditions on the basis of raindrop, radar, and synoptic weather data. The first section reviews the variability of the observed Z-R values in relation to rainfall types; the second interprets the behavior of Z-R points in terms of N_D curves; the third describes the fit-curves of N_D-D relationships proposed by the author; the last discusses the relationships between the parameters of the fitting equations and some weather conditions.

ACKNOWLEDGMENTS

INTRODUCTION

Purpose and Scope

  The manner in which the Z-R relation is modified by synoptic and physical conditions has been studied by Atlas and Chmela.[1] On the basis of data collected in Japan, Imai has drawn conclusions which emphasize the importance of evaporation.[2] The author of the present paper, using the extensive raindrop data collected by the Illinois State Water Survey, first seeks some systematic features in the variance of the size distributions of raindrops and then interprets the variances between drop sizes and the Z-R relation on the bases of physical and synoptic analyses. The present study is a preliminary stage of a larger study in which the author and other investigators at the Illinois State Water Survey are engaged.

  Discussion of drop size distributions in the papers mentioned above is based, for the most part, on the assumption that Marshall and Palmer's[3] distribution describes the initial stage of the distribution; this paper regards Marshall and Palmer's distribution as one that is the result of modification.

  This paper places special emphasis on the coalescence process, since it is thought to be the principal process in the growth of drops from cloud droplet size to rain drops of millimeter size.

Data

  The principal raindrop data used in the analyses were those taken at the University of Miami by the "raindrop camera" technique.[4] The 37 storms included in the present analyses were selected to have continuous drop size data and to have simultaneous radar pictures. However, it should be noted that not all thirty-seven storms were used in every case; only the storms relevant to each phase of the investigation were used. Furthermore, in connection with some problems additional data were used.

1. VARIABILITY OF Z—R POINTS AROUND THE REGRESSION LINE

a. General Observations

    The data used in Sections l.a., l.b., and l.c. included 11
thunderstorms, TRW; 9 rainshowers, RW; and 9 continuous rains, R*.
The data for each rain type were plotted on Z—R coordinates and
regression lines were drawn (Pigs. la, lb, lc). Comparison of
the plots yields the following general observations:

    1. The points for each plot are widely scattered.
    2. Variability of Z—R plots is greatest in TRW (Fig. la).
    3. The regions of high Z value occur in TRW (Fig. la).
    4. In convective storms — TRW (Fig. la) and RW (Fig. lb) —
        points tend to concentrate on the larger rate side of
        the regression lines.

b. Deviations of Z—R from Regression Lines

    Data containing the greatest deviation of Z from the regression
line toward the higher values of Z contained a few extremely large
drops. Drops larger than 5 mm lack the stability to be sustained
in the turbulent atmosphere.[5] Some of the huge drops exhibit a
parachute shape when photographically measured.[6] Such shape is a
transient state of the drop during disintegration.

    Drops larger than 5 mm are important, not only because of the
great deviation caused in the Z—R plot, but also because of the
deformation effect on the measuring of the drop size. If a drop,
the equivalent spherical diameter of which is 5 mm, is measured as
6, 7, or 8 mm because of the oscillatory deformation, the erratic
enhancement of Z values is 2, 5, or 10 times, respectively.

    For reference, frequencies of storms which contained such
erratic large drops are shown in Table 1. However, the effect
of these drops on the R measurement from Z values is lessened
considerably if the sample contains data for more than two minutes,
i.e., $\tilde{}2m^3$ of volume.

_____

    The symbol for continuous rains will be written as R in
this paper to avoid confusion with R (rainfall rate).

TABLE 1

Selected Storms in Miami with Large Drops

Rainfall type	Storms in which all drops had D ≥ 5 mm		Storms in which some drops had D ≥ 5 mm		Storms in which some drops had D ≥ 7 mm		Total storms
	No.	Pct.	No.	Pct.	No.	Pct.	No.
TRW	2	14	12	86	5	36	14
RW	5	50	5	50	0	0	10
R*	10	77	3	23	1	8	13

(Maximum drop size was 8.9 mm observed in TRW 10/10/57)

The standard error in R that results from a measurement of Z by means of the regression line of Z-R was investigated to evaluate the accuracy of rainfall measurement by radar. The deviations of R from the regression line were calculated for each of 35 storms. The results are illustrated in the form of frequency curves of the value of the deviation

$$\sigma_{R/\bar{Z}} = \left[\sum_{j}^{N} (\log_{10} R_j - N\log_{10} r_j)^2 / N \right]^{.5} \tag{1}$$

where r_j is the value of R estimated from the regression equation and the observational value of Z_j, and j is the identifying number given each minute's data when the minutes have been ordered chronologically. Though the instances are too few for statistical certainty, the results (shown in Pig. 2) indicate:

    1. TRW exhibit the largest diviation of R.
    2. The extreme TRW have standard deviations of +70%
        and -43% from the mean R values.

It is clear that the extremely large standard deviations from the mean R values in the instances of the TRW were caused by the large drops contained in the sample. Thus, it was to be expected that the standard deviation, as defined above, would be reduced considerably if the sampling size were increased.

To test the effect of sampling size on the observed drop size spectra

$$Z_S = (\sum_{j=1}^{1+s-1} Z_j)/S \qquad\qquad (2)$$

was plotted against

$$\overline{R}_S = (\sum_{j=1}^{1+s-1} R_j)/S \qquad\qquad (3)$$

Instead of Z_j, R_j themselves for a few cases. The results are shown in Figures 3a, 3b, 3c, and Table 2. Since each Z_j and R_j contributed only once to the series of $\overline{Z}_S$ and $\overline{R}_S$, the results show the effect of sampling size on the dispersion of the Z-R plots.* Wide scattering of Z-R points In the high Z-R region in TRW was found to be considerably reduced by doubling the size of the sample. Since the scatter was caused by the disproportionate effect of the occasional very large drop in the sample, increasing the size of the sample lessened the effect of the one drop.

On the other hand, it was quite noticeable that even when sample size was increased the scattering of Z-R points did not decrease in the low Z region as it did in the high Z region in TRW. The scatter of $\overline{Z}_S$, $\overline{R}_S$ points in low Z cannot be accounted for on the basis of insufficient sample, for the error did not decrease as the size of the sample increased.

Incidentally, the maximum sampling size taken here (S = 10) corresponds to raindrops in $10m^3$, and the horizontal dimension of that part of the cloud from which the data were taken was estimated as 600 x v meters, where v is echo velocity in meters per second.

The equation for the mean logarithmic deviations (F) listed in Table 2 is as follows:

---

*The symbol, S, is used In this section to represent sampling size. In Section 3.c, and later sections, S represents the product of the collision factor and time in random coalescence equations.

$$F = \sum_{i=1}^{N} [\log_{10} Z_{reg}(i) - \log_{10} Z_{i,S}]/N \qquad (4)$$

where Z_{reg} (i) is the Z value from the regression equation, and where $Z_{i,S}$ is the mean Z value, Z_S of the i th group of Z_j.

TABLE 2

Comparison by Rainfall Type of Mean Deviations from the
Regression Line of $\log_{10} Z_S$ for Selected Sampling Size (S)

Rainfall type and date	Mean logarithmic deviations (F) for					
	S = 1	S = 2	S = 4	S = 6	S = 8	S = 10
TRW+ 10/3/57	.156 (60)*	.166 (30)	.124 (18)	.141 (14)	.126 (11)	.148 (9)
TRW-; RW 12/23/57	.114 (86)	.100 (38)	.106 (21)	.105 (14)	.075 (11)	.100 (9)
RW 1/2/58	.121 (60)	.160 (27)	.124 (15)	.118 (10)	.146 (8)	.143 (6)

*The numbers in parentheses represent the number of groups, N, on which each mean is based.

c. Chronological Patterns of Z-R Plots

Although Z-R plots for each minute of data showed a very erratic chronological pattern, they often revealed clockwise cycles (3 to 5 minutes per cycle) in some TRW (Fig. 4). Consequently, the points dispersed widely around the regression line of the storm.

The pattern of the clockwise cycle indicated that the large drops appeared on the ground first and that they were followed by gradually diminishing sizes. Similar phenomena were studied by. Marshall[7] and Imai[8] for RW.

The clockwise characteristic depends on the cellular structure of the storms. Prom echo analysis the velocity of individual echoes for 8/28/57 was interpolated as 21 knots. Assuming that the individual small echo represented the individual cell, the horizontal dimension of individual cells composing the TRW echo was a approximately 1.0 to 1.5 miles.

As Illustrated typically by the data for 8/28/57 in Figure 4, chronological cycles of one-minute Z-R points give some indication of the cellular structure of the storm. Some examples follow:

1. 7/25/58 — 4 cycles, i.e., 4 cells, passed the station. Two cycles were clockwise (clockwise cycles are assumed to be positive; counterclockwise, negative); two were counterclockwise..

2. 8/28/57 — 6 cycles passed the station, all of which were explicitly or implicitly positive.

3. 10/3/57 — 8 cycles were recognized, but they were so nearly homogeneous that Z-R characteristics were hard to distinguish. They appear to have been as follows: 3 positive, 2 negative, 3 indistinguishable.

Both TRW which produced small and grainy, PPI radar echoes (e.g., the cell which passed from 1201-1203 EST* on 8/28/57) and TRW which produced large, superimposed PPI radar echoes (e.g., 7/25/58) produced the linear exponential type N_D curve. It may be that the well developed TRW with large, superimposed echo and raingage trace Type I (Fig. 5) had the linear exponential type N_D curve because N_D curves derived from elementary cells (such as Type III) were intermixed. Bimodal patterns are also very common in the transient periods between cells.

Analysis of TRW of the superimposed echo type (10/10/57, 3/24/58, 3/13/58) showed that the large, superimposed echo was related to the indistinguishable Z-R cycles. Raingage traces, classified as shown in Figure 5, furnished additional evidence of this relationship. Furthermore, when the Z-R cycles formed a clockwise pattern, the traces corresponded to Types II and III in Figure 5.

d. <u>Parameters of the Z-R Relation</u>

The Z-R relation is usually described as the linear logarithmic curve, log Z = log A+b log R (although a nonlinear curve has

_____

*All Miami, Florida, times are EST; all Champaign, Illinois, times are CST.

been suggested as a better fit to the overall Z-R plot[9]). Z-R points on log-log coordinates can define the regression line $Z=AR^b$ objectively. A and b thus determined are parameters which describe important characteristics of the drop size distribution. The parameters A and b were used to examine the relation of storm type, rainfall type, and other weather indices to drop size distributions.

Data used in this investigation included 31 storms from Miami, Florida, 41 storms from Champaign, Illinois,[9] 12 storms from Tokyo, Japan,[10] and 4 storms from Darmstadt, Germany.[11] Rainfall types for these data were classified as follows:

1. Miami — generally according to the observation log which was kept in conjunction with operation of the drop camera. Types were changed in a few cases on the basis of radar and synoptic analysis.

2. Champaign, Tokyo, and Darmstadt — according to the classification used by the author of each report.

Several significant relationships between regions of A, b values and various rainfall types are indicated in Figures 6a, 6b, 6c, and 6d. Figure 6a indicates that the plane can be divided into three rainfall types, though the points are considerably scattered.   *

Large A (up to 1000) and medium b (1.25 to 1.65) were found with TRW. RW resulted in smaller A and b. R* resulted in wide scatter over the range of b from 1 to 2, but the A values were generally restricted to less than 600.

The difference in TRW between two geographical regions is shown in Figure 6b. The coefficient A had lower values in Florida than in Illinois, and was less scattered in the former than in the latter. However, differences in RW and R* did not appear to be significant (Fig. 6c). Basing their conclusions *on* a greater number of raindrop data, Jones and Mueller[12] also described differences for TRW between Florida and Illinois and found that b was larger for Illinois while A had nearly the same value for both. The difference between results obtained by Jones and Mueller and

those obtained by this paper is due to a difference between methods of handling data. In this paper the total data were divided into individual storms; then regression lines were computed for each storm. Jones and Mueller, on the other hand, grouped the storms together by synoptic types and determined a single b and A for the group of storms. The results of this method indicated that many heavy rainfall TRW have very high A and relatively high b values. If these high A and heavy rainfall TRW are grouped with low A and lighter rainfall TRW, the regression line will have high b, low A values. Therefore, the many storms with high A value shown in Figure 6b contributed to the steep regression line for the overall data.

Because of the wide scatter of Z-R points on which each regression line, Z=AR , is based, questions arise concerning the significance of the relationship of one A, b point to an adjacent point. The 95 percent reliability ellipsoids (Pig. 6d) are given as one criterion for estimating the reliability of the points. Calculations for the ellipsoids were based only on the Miami data. It was assumed that the scatter of Z-R points was distributed normally around the regression line of log Z and log R — although, strictly speaking, the distribution for these data was not precisely normal. It was also assumed that log Z is independent and log R, dependent for purposes of the regression line to determine A, b. It should be noted that a large ellipsoid indicated lack of confidence in the determination of A, b.

Although the adjacent ellipsoids overlap each other, a preferred region is clearly distinguishable for rainfall types; one RW point (A=470, b=1.4l for 11/25/57) is an exception which is noted in Section 2.d. The TRW region is indicated by a broken line.

2. VARIABILITY OF N_D CURVES

a. General Observations

It is necessary to consider next the variability of N_D curves*
in relation to Z-R (Sec. 2.b.), A, b parameters (Sec. 2.c), vari-
ous rainfall types (Sec. 2.d.), and the multimodal construction of
N_D curves (Sec. 2.e.).

Data for Section 2.b. were taken from Miami and Champaign and
are illustrated in Figures 7a, 7b, 7c, 7d, and 7e. The data for
Sections 2.c. and 2.d. were also taken from Miami and Champaign
and are illustrated in Figure 8. The data for Section 2.e. were
taken only from Miami and are illustrated in Figures 9a, 9b, and
10. The appendix contains a weather summary for Miami during
times that data were collected.

b. N_D Curves and Parameters Z and R

N_D curves were found to vary greatly with relation to Z-R
values and with relation to rainfall types. The typical examples
show how much N_D curves differ when Z values are different but R
values equal (Fig. 7c) and when R values are different but Z values
equal (Figs. 7a and 7b). Figure 7e shows schematically that N_D
curves to the left of the Z-R regression line are characterized by
a wide spectrum and skewed or multimodal patterns; curves' to the
right of the regression line have inverse characteristics. Figure
7d is an example which indicates that considerable discrepancy is
usually found between two N_D curves for different rainfall types
even at identical Z-R coordinates. Relationships between N_D
curves and rainfall types are discussed below in Section 2.d.

---

*Each ND curve was plotted chronologically as data from a one-
minute sample. In this paper such a curve is called a one-minute
ND curve, where ND is the concentration of drops per unit size in-
terval. The plots were made on semilogarithmic paper; the ordinate
represents N and the abscissa, the diameter, D. Discussion of ND
curve patterns in this paper is always based on curves drawn on
this coordinate system.

C. <u>ND Curves and Parameters A and b</u>

The Z-R relation ($Z=AR^b$) was determined by calculating, with log Z as the independent variable, a regression line from log Z-log R points. N_D curves, the Z-R points of which lay on or near the regression line, were used, as being the representative N_D curve for the value of R, instead of the average one-minute N_D curves for each R. The resultant groups of N_D curves are shown on A, b coordinates in Figure 8.

Though many minor fluctuations occurred, the pattern of the curves changed in a fairly systematic manner according to A and b. Two main types of N_D curves were found: one was symmetric monomodal, represented typically by data for RW 11/27/57; the other, a skewed type with a large drop tail which trended asymptotically to a linear exponential, represented typically by the data for TRW+ 8/7/53. It is convenient to express the linear exponential type by the formula

$$N_D = N_o \exp(-\lambda D). \tag{5}$$

However, N_o changed with R, and was not always 0.08 cm as was suggested by Marshall and Palmer.[3]

The symmetric monomodal distributions were in the small A, b range; the linear exponential distributions, in the large A, medium to large b region (though a few exceptions are to be noticed). Intermediate types of distributions were represented in the data for TRW 5/13/58, RW 10/10/54, and R* 1/21/58.

Some characteristics of relationships between N_D curves and A, b coordinates follow:

1. If the N_D curve maintained the same shape on log N_D - D coordinates, and if b = 1, then the curve changed only in height with changing R. The curves for RW 1/23/58 and R* 10/26/53 approximate this relationship.

2. The mean diameters increased with A; compare curves for RW 1/23/58 and R* 10/26/53.

3. When the mode diameter increased with rainfall rates, b

became larger than one, as in R* 8/8/54 and RW+, R*
5/23/58. The mode diameters of the curves at R = 1 mm/hr
must increase with A. In the following instances slight
differences between even the smallest curves can be rec-
ognized; compare R* 8/8/54 and RW 11/27/57 or RW 12/26/57
and RW 11/27/57.

4. Further increase of b was attained with changing spectrum
   widths. Marshall and Palmer's expression can be applied
   to this type.

5. Extreme values of b were attained by a shift of the mode
   to the right and a lowering of the peak height with an
   increase in R.

6. Large A, large b were usually found with heavy TRW whereas
   small A, small b were found with light RW and R*.

d. ND Curves and Rainfall Types

The N_D curves in Figure 8 have been divided into rainfall
type regions by broken lines. For purposes of this division, a
brief analytical study of synoptic maps, drop camera data, and
radar film was made for 33 storms of Miami data. The results are
given in Appendix.

Figure 8 indicates that the linear exponential type (or low
s value of the fitting curve, which is proposed by the author as
Eq. 6 in Sec. 3.a.) is generally found with TRW and moderate to
heavy R*; the symmetric monomodal type (or high s value) is found
with light RW and light R*; the mode shift is found with R*.

Although the evidence available from synoptic maps and radar
films was inadequate for clarifying the small scale structure of
the storm, the results of the analysis were generally suggestive
of a consistent physical reason for the N_D types. Among RW and
R* the less intense cases occupied low A, low b regions and had
symmetric monomodal N_D curves. The aerological situations for
RW 11/25/57 and RW 11/27/57 were nearly identical; there were
positive convective stability layers at 750 and 800 mb, respec-
tively, but the convective cell producing the raindrop data was

weaker and less developed in the latter. The RW was a type of
warm rain.* The cold frontal storm of 11/25/57 developed from
an updraft and had a dry environment. The relatively strong up-
draft and evaporation of falling drops caused the A position to
move to the TRW region, even though the storm was not accompanied
by evident thunder activity. Synoptic and radar evidence showed
the R* of 3/19/58 and 2/7/58 to have been associated with elevated
generating cells. Generally, the wide spectrum was found in a
storm which consisted of bulky or wide convective echoes, e.g.,
squall lines.

e. <u>Multimodal Construction of ND Curves in TRW</u>

Each N_D curve in Figures 9a and 9b was drawn from a one-minute
sample of Miami TRW. The two examples of chronological change of
N_D curves (Figs. 9a and 9b) show how the wide spectrum was made.

While the core of the TRW echo (Fig. 9a, 5/13/58) was passing
(1425-1432), N_D curves indicated reductions in the entire drop
size range, but the number of drops in each class decreased with
time. A different pattern occurred from 1436 to 1444. At 1436 a
few 4-mm drops were observed; at 1440 the number grew and produced
independently of the change in the smaller mode (near 1.5), a
second mode (near 3.5).

Two developments of linear exponential N_D curves were observed
for 7/25/58 (Fig. 9b) from 1605 to 1623. Best development occurred
at 1619 to 1620. Just previously, at 1613, only a few large drops
appeared; the following minutes showed increases in the small and
medium drop ranges.

The change of N_D values at medium to large drop size (1 to
2 mm) was usually independent of the change in the small size mode,
e.g., 1605 to 1606. These features suggest that the one-minute
curves for this storm consisted of at least two modes; one, about
1 to 2 mm in diameter; a second, about 3 to 4 mm in diameter.

─────────────────────────

*Radiosonde data indicated the top of the cloud layer developed
at a point below the melting level.

Raingage traces were taken of the storms from which the rain-drop camera obtained the data herein considered. The traces re-vealed the cellular structure of the storms. Figure 10 illustrates the relationship between A and b in terms of the raingage tracings: circles indicate amalgamated cellular structures; triangles, sepa-rated cellular structures. Numbers within each figure represent raingage trace classifications (Pig. 5). Figure 10 shows that amalgamated cellular structure is related to high A, b values of N_D curves. Figure 4 and the evidence presented in Section 2.c. indicate that the characteristics of the Z-R points are related to the characteristics of the cellular structure of the storm. PPI echo pictures indicate that the linear exponential form was caused by the amalgamated cellular structures — further evidence of multimodal construction of N_D curves in TRW.

3. THE PROPOSED FITTING EQUATION: ITS RELATION TO THE ONE-MINUTE N_D CURVE AND ITS PHYSICAL MEANING

a. The Proposed Fitting Equation

Several previous investigators have proposed fitting equations for N_D curves: Marshall and Palmer,[3] Blanchard,[13] and Best,[14] among others. The equation proposed by the author is intended to have application to a, greater variety of N_D curves than have those equations previously proposed.*

As indicated in Figures 8 and 9a and 9b, one-minute N_D curves change not only their mean, mode size, and number but also their skewness. The following empirical formula is proposed to express such a skewed curve:

$$1 - [\sum_{}^{D} N_D \Big/ \sum_{}^{\infty} N_D] = \exp[-\{(D-D_o)/a\}^s] \qquad (6)$$

where a, D_o, and s are the parameters related principally to the

---

*The primary purpose of the application is to analyze ND curves in relation to the physical aspects of a cloud. Further, a flexible and improved expression for practical use is now being developed under this contract by E. A. Mueller.

magnitude of the broadness, mode, and skewness, respectively. The curve patterns expressed by the equation are illustrated in Figure 11 (compare Pig. 8). The value of s usually varies from 1 to 3. The curve patterns indicate that when s = 1 the equation is equivalent to the form proposed by Marshall and Palmer.[3] When s = 3 the equation also expresses the random coalescence distribution which is defined by Equation 12 (Sec. 3.c.). Furthermore, these two typical cases represent the extremes observed in convective storms.

In rain, D_o does not diminish as the coalescence equation indicates it will. The average of D_o was approximately 0.8 mm (physical interpretation is given later).

Figure 12 contains several examples of curve fitting by Equation 6. D_o is substituted by the cut-off size in the left side of the curve. $\mathbf{Y = \log \left[-\log_e \left\{1-\left(\overset{D}{\Sigma} N_D \middle/ \Sigma N_D\right)\right\}\right]}$ was taken on the ordinates and X = log (D-D_o), on the abscissas. The intersection with the Y = 0 line gives us log a, which varies from 0 to 0.5. Namely a = 1 to a = 3.5.

The relatively poor fit in the case of 7/25/58 will be due to an uneven composition of the elementary curves, and of two dominant modes. (See Sec. 2.e.) If allowance is made for the variability of N_D curves, the equation represents the data quite satisfactorily. In Figure 13, the distribution of s values in convective storms is shown in A, b coordinates. The tendency of the s values is shown as a function of A and b by the crudely drawn contours.

Although both Marshall and Palmer's and Best's equations are intended for average size distributions rather than for those taken from individual observations, both are comparable to Equation 6 in some cases. Marshall and Palmer's is comparable to Equation 6 in cases of TRW or heavy R*, Best's is more nearly comparable in a greater variety of cases than Marshall and Palmer's is. However, Best's equation is not comparable for that portion of the curve where the drop size range is less than the mode; this particular difference in applicability is thought to depend not

only on different sampling periods but also basically on the method
of obtaining data. The data for the analysis of N_D curves in this
paper were obtained by raindrop camera.[4] The N_D curves for rain-
drop camera data usually fall sharply on the left before reaching
the measuring limit (0.5 mm). Data obtained by this method does
not include counts of fragments produced by splashing.

b. Definition of the Elementary ND Curve

     Although the N_D curve for a one-minute sample varies errati-
cally with time, the elementary N_D curve can be defined as a
quasi-symmetric monomodal curve drawn on coordinates which repre-
sent logarithmic concentration and diameter of drops, when s = 3
in the fitting equation (Eq. 6). When s is smaller than three,
the curve is considered to be primarily a composite of the elemen-
tary curves. To verify the composition, a representative fitting
equation with two parameters was defined by substituting $D_o = 0$,
s = 3, in Equation 6:

$$N_D dD = \alpha D^2 \exp(-\beta D^3) dD \qquad (m^{-3} cm^{-1}) \qquad (7)$$

where D is the diameter in cm, and α and β are the parameter
constants dependent on the case. The most frequent discrepancy
in N_D plots made from Equation 7 was the shift of mode. Accord-
ingly, all of the monomodal N_D curves were fairly closely expressed
by

$$N_D = \alpha (D-D_o)^2 \exp[-\beta(D-D_o)^3] \qquad (8)$$

where D_o is as defined in Equation 6. The amount of the mode
shift, D_o, is regarded basically as the quantity of drop size
growth by accretion (see Sec. 3.c).

     The displacement of five Z-R points made during the shift,
$D_o = 0.5$ mm (a common magnitude), is shown by open arrows (Fig. 14).
The magnitude of this shift will correspond to an effect of accre-
tion attained with 10-km fall through a cloud with 1-gram/m^3

effective water content (or 5-km fall through a cloud with a 2-gram/m^3 effective water content), where effective water content is total liquid water content of the drops multiplied by the collection efficiency. Figure 14 also indicates that the mode shifts of N_D curves change Z values along the b = 1.7 slope, as long as magnitude of D_O does not exceed 0.5 mm.

c. Physical Meaning of the Fitting Curve

Continuous increase in the diameter of drops through accretion and condensation changes the N_D curves. Assuming N_D to be a function, f (D,H), of diameter, D, and altitude, H, the change rate of the size distribution function can be expressed as follows:

$$df(D,H)/dt = \partial f(D,H)/\partial t + div[\overline{V}_D \cdot f(D,H)]$$

$$- \partial[f(D,H)dD/dt]/\partial D \tag{9}$$

where $\overline{V}_D$ and dD/dt are the velocity vector of the drops of diameter D per unit diameter interval and the growth rate of drops, respectively. The left side of the equation represents the change by coalescence and disintegration. The three terms on the right side of the equation represent spatial change, mixing and sorting effect, and effect of continuous drop diameter increase (by evaporation, condensation, and accretion), respectively. If Equation 9 is divided by the fall velocity of drops, V_D, (which is a function of drop diameter, D,), the rate of change of the distribution function with regard to height is obtained;

$$df/dH \equiv (df/dD/V_D = \partial f/\partial H + V^{-1} \cdot div(f \cdot \overline{V}_D)$$

$$- V_D^{-1} \cdot \partial (f \cdot dD/dt)/\partial D. \tag{10}$$

If the drop size distribution is assumed to have been observed inside the cloud, the effect of heterogeneous mixing and sorting can be assumed to be negligible as compared to other phenomena.

Then Equation 10 can be rewritten as

$$\partial f/\partial H \equiv (\partial f/\partial H)_1 + (\partial f/\partial H)_2$$

$$\tag{11}$$

$$= (df/dt)/V_D + V_D^{-1}\partial(f \cdot dD/dt)/\partial D.$$

Although analytical integration of Equation 11 is complicated, a rough evaluation of each term can be given as follows:

Coalescence — Several investigators in colloidal chemistry have assumed a closed system, and have solved the coagulation equation of colloidal particles (random coalescence equation). The following is the solution given by Melzak and Hitschfeld.[15]

$$N_D dD = N_m d_m = \alpha' \exp(-\beta' m)dm, \tag{12}$$

where $\alpha' = 4/S(SN+2)M$, $\beta' = (1/M)\log_e(1+2/SN)$ and where m is the mass of drops, S, the product of the collision factor and time elapsed since coalescence began at homogeneous particle sizes; M, the mass of initial particles; and N, the initial concentration of particles. This equation is identical with the elementary fitting curve (Eq. 8), defined in Section 3.b. The assumption of a closed system for this theory probably holds good approximately in the center of convective cells.

The effect of the initial characteristics of the distribution on the resultant distribution will decrease with the development of the coalescence process.[16] The coalescence coefficient is usually defined as

$$C_{ij} = E_{ij}S_{ij} |V_i - V_j| \tag{13}$$

where E_{ij} and S_{ij} are the Langmuir coefficient and sweep cross section for drop i and drop j, respectively; V_K is the fall velocity of the drop, K; and C_{ij} is approximated by the value proportional to the difference between the mass of the two drops, i and j. However, in the atmosphere, coalescence may actually occur even between drops of the same mass; such coalescence depends on

turbulence, deformation of the shape of drops, and electrostatic effects. This fact supports the assumption that C_{ij} = constant can be applied for the first approximation to natural coalescence.

Accretion — The second term of Equation 12 represents principally accretion growth within the active cloud. In the early-stages of drop growth the coalescence equation accounts for accretion of cloud droplets. As the drops grow larger, the drop concentration is reduced and therefore the coalescence rate per unit of height decreases. Thus, in the later stages the accretion of cloud droplets becomes a more important process than coalescence. Therefore, the two terms of Equation 11 can be integrated separately with an approximation in the right side. Thus,

$$(\partial f/\partial H)_2 = -\partial(f \cdot dD/dH)/\partial D, \qquad (14)$$

where $\quad dD/dH = \overline{V}_D^{-1}dD/dt$

and V_D is the mean fall velocity of drops around the mode, and where dD/dH varies not only with the collision factor but also with cloud droplet distribution and updraft. Under certain conditions (e.g., when the updraft is low compared with terminal speed of the raindrops) dD/dH is approximately constant, and the solution of Equation 10 becomes

$$f(D,H) = N_D(D-CH). \qquad (15)$$

If D_o is substituted for CH, Equation 15 becomes the same expression as Equation 6, i.e.,

$$1 - (\overset{D}{\Sigma} N_D / \overset{\infty}{\Sigma} N_D) = \exp[-(D-CH)^3/a^3] \qquad (16)$$

Thus, it is concluded that mode shift of the N_D curve (D_o as defined in Sec. 2.b.) is explained by the accretion growth of drops. Since the updraft emphasizes the shift in smaller sizes, curves will skew slightly towards smaller sizes as is often seen in curves drawn from actual data.

Evaporation — The effect of evaporation of drops on N_D curves can also be calculated by Equation 14. The results also depend on N_D curves $N_D = f(H,D)$. The dD/dH is approximately proportional to the inverse in D; the tendency of the decrease depends on the dryness of the evaporation layer, though the precise relationship is very complicated.

The effect of evaporation on N_D curves is extremely significant when rain fails through a thick arid layer. The importance of evaporation has recently been discussed by Imai,[2] who made use of calculations based on actual weather conditions. However, when average humidity is greater than 85%, when average drop size diameters are greater than 0.8 mm*, and when the evaporation layer is less than 2 km, coalescence has much more effect on drop size distribution than evaporation has. The conclusion is that the symmetric monomodal N curves commonly observed in RW may be fitted by Equation 16, which can be obtained theoretically by use of random coalescence and accretion processes.

4. FACTORS WHICH GOVERN DROP SIZE DISTRIBUTIONS

a. General Observations

The final section of the paper discusses various factors which govern drop size distributions. Sections 4.b. and 4.c. discuss the Z-R relation and random coalescence; Sections 4.d. and 4.e. discuss condensation nuclei and moisture in relation to drop size distributions; Section 4.f. contains additional notes on coalescence and on analysis of the Z-R relation. Data are drawn from Illinois and Florida and are illustrated in Figures 14 and 15.

---

*In the data used for this paper minimum D for N_D plots ranged from 0.5 mm to 1.5 mm; the average was about 0.8 mm. Environmental humidity below the cloud base before the beginning of the rain was greater than 75% for this data except for the following cases: 10/25/57, 11/21/57, 1/7/58, 1/23/58, and 2/7/58.

b. Z-R Relation as Determined by Random Coalescence Equation,

A storm is usually composed of multiple convective cells, each of which generally requires at least three minutes to pass over the raindrop camera. Echo traces on photographs taken at five-minute intervals indicate that most passing periods are no longer than one-third of the life cycle of individual bubble activities. Therefore, the data from a chronological cross section observed at a fixed station can give a picture (as a first order approximation) of the horizontal one-dimension cross section; however, when the cells pass very slowly the above conclusion no longer holds true. Therefore, the regression line for each storm was assumed to express an average relation between the drop size distribution and the various stages of development of the cells which were composed along the cross section of one storm.

Further, even in the case of the skewed type of N_D curve, the N_D curve of random coalescence was used to discuss the primary effect of coalescence on the Z-R relation.

To compare data with the idealized process (random coalescence), Z and R were calculated by means of Equations 12, 18, and 19 and the formula for the approximate terminal velocity of raindrops,

$$V = 1400 \sqrt{D} \tag{17}$$

where V and D are in cm/s and cm, respectively:

$$R = \int_0^\infty N_D (\pi/6) D^3 \times 3.6 \times 14 \sqrt{D} \cdot dD \tag{18}$$

$$Z = \int_0^\infty D^6 \, N_D dD \tag{19}$$

The results are

$$R = 9.5 \times \alpha' \beta'^{-2.167} \tag{20}$$

$$Z = (2/3 \times 10^6 \times \alpha' \beta'^{-3} \tag{21}$$

where α', β' are given by the solution of the random coalescence equation (Eq. 12). Using an approximation

$$1 \gg 2/SN, \quad SN \gg 2 \qquad (22)$$

and assuming that the mass of one initial particle is $M = 10^{-7}$ gram, i.e., the initial diameter particle is D = 56.7 microns where the density of the particle = 1, the following relationships are obtained;

$$R = 3.68 \times 10^{-7} S^{0.167} N^{1.167} \quad (mm/hr) \qquad (23)$$

$$Z = 3.64 \times 10^{-8} SN^2 \quad (mm^6/m^3) \qquad (24)$$

The calculations performed in Equations 23 and 24 are illustrated by the diagram shown in Figure 14.

The assumed initial size of the drop seems reasonable when compared with data for droplets observed from clouds and when compared with the size, discussed by theoretical investigators as the threshold size, from which drops grow rapidly by coalescence.

c. Variability of the Z-R Relation on the Coalescence Diagram

Figure 14, which is a diagram of the random coalescence progress, shows the result of calculating the theoretical Z-R relation in terms of the number/m^3; S is expressed in terms of times of collision per one drop per cubic meter during the fall. Figure 14 also shows the region of distribution of Z-R points for Miami data and three regression lines: highest b, dated 2/7/58; lowest b, dated 1/23/58; and the mean, labeled "Mean of Miami."

It should be noted that the regression lines for convective storms lie between S = constant and $N^{.5}$ S = constant. The high – Z values in heavy rainfall in TRW occurred in the huge drop region (shown by -.-. in Fig. 14). The heavy rainfall rates are accompanied not only by the increase of initial concentration N but also by the increase of coalescence factor S. The figure also shows that no heavy rainfall occurred in which N decreased or

held constant while rainfall intensity increased, N changed by 10^2 when intensity increased from drizzle to heavy rainfall (N = 10^8 at $2^{mm/h}$; N = 10^8 at 200 mm/h per cubic meter); S, on the other hand, increased only by one order of magnitude. The . sensitivity of N with respect to R is probably due to the term, N^2, in the coalescence equation. The wide range of N can be due to the variability in the concentration of condensation nuclei and other mechanisms of precipitation.

Since S = Ct (assuming C to be the collision factor in random coalescence), S increases with the relative fall depth which is approximately as follows: H - (V_D - W)·t, where W is the speed of updraft; therefore, relative fall depth increases with updraft intensity. Since the actual collision factor is approximately the average value of Langmuir's coefficient, multiplied by swept cross section, multiplied by fall velocity difference, the equivalent value of C increases rapidly with an increase in the average size of drops and the width of the spectrum. Therefore, the constant-height, i.e., the line of constant relative fall depth, must have much less slope than that of S = constant.

The discussion thus far in this section has assumed an ideal coalescence process, If other processes are intermixed, more complicated variability can be expected. When accretion beneath the generating cloud is the primary cause of change in Z-R, the slope of the regression line is relatively high, e,g,, it was estimated to be 1.7 by means of the simplified calculation described in Section 3.b.

Although a regression line with a slope steeper than 1.7 can be attained theoretically for an S increase and a lesser increase of N by coalescence alone, most of the regression lines with a slope steeper than 1.7 were actually attained by a combination of different mechanisms or by the sorting process for which the assumption of an ideal closed system does not hold. This indicates that an S increase is always accompanied by dN/dR, probably because of disintegration of large drops and the first mechanism described in

Section 4.d. If sublimation growth and snowflake coalescence with a high value are accompanied by an R increase, and if the warm type of rain mechanism is superimposed in the low R portion of the plots, the regression line with extremely high b values will result. Such a high b regression line is to be expected also when there is weak convective activity in the freezing layer just above a stratified cloud layer of the type which would produce warm rain.

d. Raindrop Size Distributions and Condensation Nuclei

Each of the multiple cells of a storm defines a regression line and has both droplets started at the condensation level and precipitation from the generating level that will be determined by the cell's stage of development and activity. Consequently, the concentration of the precipitable drops generated, N, changes with every convective cell according to its activity and controls the drop size distribution as well as the Z-R relationship observed on the ground.

A comparison of N values on the order of .1 to $100/cm^3$ (Fig. 14) with the concentration of cloud droplets observed by Diem[17] and Weickmann and Aufm Kampe[18] showed that the initial concentration of raindrops was less than the total of all cloud droplets from a common hygroscopic nuclei. The principal reasons for the extensive change of N with every convective cell follow:

Coalescence growth of droplets accompanied by condensation growth — Theoretical calculations have tended to deny that cloud droplets grow to drizzle size by condensation alone within an acceptably short time. Numerical calculations made by East[19] have emphasized the possibility of drizzle growth by condensation and coalescence simultaneously when liquid water content is high enough. This conclusion seems reasonable because coalescence increases in proportion to the increase of N^2 and N may increase with moisture if there is a sufficient concentration of hygroscopic nuclei. Sufficient moisture supply makes possible the increase in the concentration of activated droplets and also of precipitable drops.

Giant hygroscopic nuclei — It is accepted that giant hygro-
scopic nuclei are the most important cause for RW when cloud tops
do not reach the freezing level for drops. Rainfall is coordinate
in low A and low b regions of the giant hygroscopic nuclei type.
The case dated 10/26/53 (Pig. 8 with b as low as one) was warm
front type rain and was composed of drizzle or light R*. During
the time that the generation level remained nearly constant, the
changes in the drop size distribution were most sensitive to the
N increase. Theoretically, Bowen's[20] and Ludlam's[21] warm rain
mechanisms for a layer cloud are likely to correspond to the case
of R* at low b because N changes while the thickness of the cloud
remains constant. In such a case the height of the peak of the
N_D curve changes while the mode remains the same.

From aerological data recorded at Rantoul, Illinois, the
level of the cloud top for the case in Figure 8 dated 10/26/53 was
evaluated at around the freezing level (700 mb) during the obser-
vation of raindrops. Although there was no evidence for doubting
the existence of ice crystals on the cloud tops, the drop sizes
were such (less than 1.5 mm) as could have been attained without
an efficient ice phase growth (cloud thickness was more than 2.3
km).

When the convective activity is appreciably intense, it is
difficult to explain the variance of N by as much as $1C^2$ (Fig. 14)
as a result of inhalation of the giant nuclei under the same wea-
ther synoptic condition. In such an instance the mechanism of
condensation in which a strong updraft with plentiful moisture
supply in conjunction with a super-cooling effect governs the N
increase in the cloud is a more likely mechanism than the growth
by giant hygroscopic nuclei. However, more quantitative study
and cloud data are needed to describe this relationship accurately.

e. Raindrop Size Distributions and Moisture
It is obviously true that the number of elementary precipi-
table drops depends, not only on the number of activated droplets,

but also on the size distributions of those droplets. Calculations
made by Howell[22] and by Neiburger and Chien[23] show that drops which
grow only by condensation develop toward a uniform size. East has
shown that, if condensation and coalescence occur simultaneously,
development of a uniform drop size would not normally be expected.
If the droplet sizes just after condensation tend toward uniform-
ity, the high concentration of droplets will actually break the
colloidal stability. Then the concentration of droplets, rather
than size of the individual droplets, will be more important in
determining the concentration of precipitable drops.

The quasi-inverse relation between A and the mixing ratio
implies (Fig. 15) that the activation rate of hygroscopic nuclei
increases with the rate of moisture supply at the threshold super-
saturation stage.

The static atmospheric situation indicates rather strongly
that surface air has the lowest level of free convection defined
by the adiabatic process. Radiosonde soundings show that atmos-
pheric layers at 700 mb or lower are often very dry during TRW
activity and that air particles at 80C to 900 mb have only slight
negative convective energy. The suction of surface air will occur
readily once the storm has developed, for the cold air of a down-
draft undercuts the warmer surface air. Therefore, it is reason-
able to examine surface air moisture as one factor in convective
precipitation.

The values of A for Florida and Illinois were plotted against
the mixing ratio (Fig. 15). The mixing ratio for Miami was ob-
served at 950 mb at Miami International Airport, and plots were
made of data both from 950 mb and from the surface which were
nearly equivalent. The mixing ratio for Illinois was observed
at the surface just prior to the storm. The thick cluster of
points on the lower right side of the figure indicates that A
values increased as the mixing ratio decreased. However, many
Illinois points were scattered over the left side of the figure;

raingage traces revealed that many of them were accompanied by stratified rain.

Two instances of the Illinois and Florida data were not readily comparable because differing mean rainfall intensities suggested different precipitation mechanisms. The mean rainfall intensities are given in mm/hr for each point in Figure 15.

Moisture supply seems to be a much less significant factor for A in Illinois than for A in Florida,

f. <u>Notes on the Application of Coalescence Diagram to Z-R Analysis</u>

Hailstone growth and break-up of large drops within the cloud are phenomena which must be considered in interpreting raindrop size distributions. When large drops break up during the fall, some of the resulting small drops may be blown to the upper part of the cloud by updraft, while the larger of the resulting small drops may continue to fall through the updraft. In either case the effect on the original drop size distribution will be to shift the Z-R regression line toward the right — the amount of the shift depending on the number of large drops and the types of distribution which occur when they break up. This modification is more or less equivalent to that made by N increase.

If moisture increases and there is a sufficient supply of hygroscopic nuclei, the concentration of precipitable drops, N, will obviously increase.

Since moisture is less significant in determining A in Illinois than it is in determining A in Florida (as shown in Section 4.e.), the fact that A values for TRW in Illinois are higher than for those in Florida seems to be due to some factor other than liquid content. Jones and Mueller,[12] on the basis of climatological data, attributed it to melting hailstones. If small drops result from the melting of the hailstones, an N increase and S decrease, i.e., an A decrease, will be observed.

Many cases of ice phase growth of precipitation, whether hailstone or snowflake, may be contained in the plots of Illinois

data in Figure 15. When freezing nucleation and sublimation growth take place mainly in the early stage of particle growth, the inverse relationship between moisture and N may no longer hold. Since many of these cases may be contained in the plots in Figure 15, they disturb the clarity of the relationship between N and moisture. Thus, the present analysis, though incomplete,. tends to agree with the conclusion reached by Jones and Mueller.

Although the analysis of the pairs of parameters (A, b and S, N) on the coalescence, diagram given by the author is limited in its capabilities for analyzing complicated phenomena such as. severe storms (TRW), it does show the variability of the Z-R regression line in terms of N and S for simpler cases. Further analysis of secondary factors which govern the values of N and S is the next step to be taken. Thus, the relationship between N, S and A, b is summarized in Table 3 by a comparison of Figures 7e and 14.

TABLE 3

Effect of N and S on A and b

Parameters	Effects	Rain Type
High A and Low b	dN/dR is high. Updraft is strong.	RW, TRW
Low A and Low b	dN/dR is sensitive to high updraft. Updraft is weak.	R*, RW
High A and High b	dN/dR is not rapid, but high S is attained by strong updraft. Raindrop heterogeneity is due to seeding from penetrating bubble, hail, and ice particles.	TRW
Low A and High b	dN/dR is not high. Raindrop heterogeneity is due to sorting during the fall from an elevated cloud, or, possibly, to accretion in lower cloud layer.	R*

APPENDIX

Summary of Weather Conditions for Miami Data

This appendix summarizes weather conditions for 30 days during which Miami data used in this paper were collected. The summaries are given in tabular form according to the following key:

1 = Times, EST, during the day when data were collected.

2 = Values for the parameters A and b for that data.

3 = Synoptic type and surface pressure pattern; the location of the pressure system is given on the basis of the 0900 map unless otherwise specified.

4 = Direction and speed of surface wind.

5 = Upper air pressure pattern or wind field; the location of the pressure pattern is given on the basis of the 0600 map unless otherwise specified.

6 = Jet stream (speed greater than 55 mph); all description of the aerological situation at Miami is based on soundings taken at Miami International Airport between 0600 and 0700.

7 = Raingage trace pattern (Pig. 5).

8 = Static stability of atmosphere.

    a. Level of free convection (LPC)

    b. Temperature differences (observed at 300 mb and at 500 mb) between the environment and the most unstable parcel of air (i.e., the parcel having the highest pseudo-wet bulb potential temperature) rising adiabatically to these levels.

9 = Wind shear (⇗at 500 mb minus⇗at 850 mb).

10 = Dryness of environmental air (ATW=T-TW at 500 mb).

11 = Description of echo pattern.

12 = Rain type.

13 = Notes

8/28/57

(1) 1048-1052; 1125-1135; 1148-1227.   (2) A = 364; b = 1.34.
(3) Easterly wave; a weak stationary NE-SW trough near Miami.
(4) E, at 5-8 mph.   (5) Flat gradient over the Gulf of Mexico;
one small closed low moved to the west.   (6) None.
(7) Type II.   (8a) 850 mb;   (8b) 6.5°C; 6.6°C.   (9.) SW,
at 5-8 mph.   (10) 3.0°C.   (11) A short rainband (ENE-WSW)
with a small echo assembly.   (12) TRW+ at noon.   (13) This was
a typical case of raingage trace Type II (Fig. 5) described in
Section l.c. The one-minute raingage trace reading and the camera
data indicated three- to five-minute cycles in rainfall intensity.
These cycles imply the bubble structure of the TRW. The cycle
was not evident for the period of steepest raingage trace; the .
very high rainfall rate continued for 17 minutes without change.
The author wishes to call this stage the amalgamated cell or echo.
N_D curves in this stage were of the linear exponential type rather
than of the symmetric and monomodal type.

9/19/57

(1) 0839-0850; 1134-1148; 1205-1223.   (2) A = 228; b = 1.34.
(3) Airmass; the southwest edge of a weak subtropical and maritime
high.   (4) E-SE, at 5-14 mph.   (5) A weak low above the
300-mb level over the Gulf of Mexico and Cuba; a flat gradient and
weak wind.   (6) None.   (7) No appreciable trace.
(8a) 910 mb.   (8b) 5.0°C.; 7.0°C.   (9) NW, at 5-14 mph.
(10) 4°C.   (11) No radar data.   (12) RW.

10/2/57

(1) 1758-1813.   (2) A = 315; b = 1.30.   (3) Pre-cold frontal;
a slowly moving cold front at the northern end of the Florida pen-
insula.   (4) Almost calm (E).   (5) A trough developing along,

or to the west of, the west coast of the United States, a gentle
ridge over the eastern Gulf of Mexico.   (6) None.   (7) Type
IV (perhaps a small Type I).   (8a) 830 mb.   (8b) 3.0°C; 3.0°C.
 (9) W, at 5-8 mph.   (10) 1.4°C.   (11) Superimposed echoes
passed the station in the southwest part of the echo; the echo
was diffuse in the northeast part.   (12) TRW.

10/3/57

 (1) 0917-1037; 1512-1522.   (2) A = 490; b = 1.34.   (3) Pre-
cold frontal; as the cold front dissipated, it moved very quickly
through Florida.   (4) Almost calm (SE).   (5) Eastern edge
of stationary N-S trough at 700 mb-150 mb; wind SSW-SW.
 (8a) 830 mb.   (8b) 3.5°C; 3.5°C.   (9) SW, at 12 mph.
 (10) 1.8°C.   (11) A convective echo embedded in a superimposed
echo passed the station as a part of the northern edge of the echo.
The diffused portion of the echo was blown toward the north.
 (12) TRW.   (13) A comparison of drop size distributions for
10/2/57 and 10/3/57 revealed that the latter had a much greater A
value than the former, while b values were nearly equal for the
two. The synoptic weather situation and PPI echoes were very
similar, but the part of the echo which passed the camera station
was different. The large A value which accompanied the diffuse
echo can be explained by a large S (coalescence factor; see Sec.
3.c.) in the ice phase of cloud development.

10/7/57

 (1) 0929-0942.   (2) A = 126; b = 1.52.   (3) Overrunning
with a weak stationary front (indistinguishable from the air mass
shower type).   (4) NE, at 9-14 mph.   (5) Southwesterly wind;
weak pressure gradient at 700 mb-150 mb.   (6) None (40 mph at
200 mb).   (7) Type V; however other raingage stations around
Miami recorded Type II or Type III in heavy RW or TRW.

(8a) 840 mb.   (8b) 1.3°C.; 5.7°C.   (9) SSW, at 9-14 mph.
(10) 23.5°C.   (11) No radar observations.   (12) RW.

10/10/57

(1) 1230-1338.   (2) A = 240; b =1.53   (3) Cold frontal:
southwest edge of the front moved slowly to the southeast; large
high in the central United States.   (4) N, at 5-8 mph.
(5) Wind WSW, at 32-49 mph, above 500 mb over the mid-south
United States.   (6) None.   (7) Type II (and Type VI).
(8a) 920 mb; however, a weak stable layer at 700-600 mb and a
moist layer beneath the stable layer indicated the existence of
stratus type clouds.   (8b) 4.7°C.; 7.5°C.   (9) NW, at 6 mph.
(10) 20°C.   (11) Widely spread echo.   (12) TRW.   (13) A
stratified rain storm was probably combined with the TRW. The
value of A is near the bottom of the TRW region (Fig. 8), but the
N_D curves are of the skewed type because the stratified cloud
(evaluated to have been near 800 mb) precipitated a number of
small drops (about 1 mm in diameter) which were measured with
the large drops from the TRW cloud.

10/25/57

(1) 1213-1237; 1548-1605.   (2) A = 129; b = 1.76.   (3) Weak
cold front; a large high developed over the northern United States.
(4) Weak winds varied from SE and SW to N as the cold front passed.
(5) WSW wind.   (6) Greater than 61 mph; WSW above 300 mb.
(7) Weak Type V.   (8a) 880 mb and 680 mb.   (8b) 2.0°C.; 1.7°C.
(9) WSW, at 10 mph, to NW, at 6 mph.   (10) 11°C. at 1900; 5.3°C.
at 0700.   (11) No radar observations.   (12) RW- at 1200;
RW — at 1600.   (13) An evaluation of the sounding indicated
that the rain cloud layer was below 600 mb (20°C.) at 0700 and
below 700 mb'[4] (8.0°C.) at 1900. Except during the morning, the
rain was evidently a warm type rain, but relatively large b was

attained by mode shift of the N_D curve toward large drop diameters
and an accompanying decrease in the amplitude of the N_D peak.

11/12/57

(1) 1251-1303; 1351-1505.   (2) A = 244; b = 1.39.   (3) Over-
running; southwestern edge of a large high centered over Virginia;
a stationary front across Cuba.   (4) ENE-NE, at 20 mph.
(5) Weak high pressure below 500 mb; a weak WSW wind above that
level.   (6) Above the tropical tropopause, at 86 mph.
(7) Type III.   (8a) 890 mb.   (8b) 4.0°C; there was a deep
and sharp inversion (780 mb; 6.5°C. at the base of the layer),
through which no convection could penetrate.   (9) E, at 32-37
mph; this difference holds true between the top and base of the
inversion layer.   (10) 16.5°C.   (11) A rainband composed
of a line of small echoes moved slowly E, at 14 mph. The small
echoes passed by E, at 20 mph.   (12) RW and R*.   (13) Quasi-
symmetric monomodal N_D curves developed the width of the spectrum
with increase of rainfall intensity. The storm was evidently
from warm type clouds. The cloud tops should have been restricted
by the inversion. The drops were formed by the coalescence pro-
cess in the water phase.

11/20/57

(1) 1135-1138; 1624-1629.   (2) A = 288; b = 1.32.   (3) A
cold front from a large occluded depression over northeastern
Canada.   (4) Weak N winds on the north side of the front; weak
S winds on the south side of the front.   (5) WSW-SW wind, but
a divergent pattern.   (6) 72-77 mph at 200 mb; 55-60 mph at
250 mb.   (7) Type III.   (8a) 840 mb.   (8b) 3.2°C.; 4.6°C.
(9) NNW, at 17.5 mph.   (10) 23.5°C.   (11) A broken line of
small echoes oriented NE-SW, moved by at 8.6 mph.   (12) RW-.
(13) The small A, large b values were obtained, even though the

radar echo and synoptic situation were very similar to those for 11/25/57 when a large A value was obtained; however, the regression line for 11/20/57 was based on only nine points taken from the two cells which passed the station (and one of these cells was very weak). RHI photographs showed several high columns (as high as 10,000 m) as well as many low ones (3000 m). The morning sounding showed one stable layer below the freezing level at 600 mb.

11/21/57

(1) 1107-1255.   (2) A = 288; b = 1.32.   (3) Overrunning; high pressure covered the southeastern coast of the United States; a cold front from a large occluded depression over northeastern Canada extended through Newfoundland, between Miami and Cuba, into the Gulf of Mexico.   (4) NE, at 2 mph below the inversion; SW, at 1-2 mph just above the inversion.   (5) SW wind.
(6) Above 300 mb.   (7) Type III; Type VI later.   (8a) 830 mb.
(8b) $2.7°C$; $1.8°C$.   (9) SW, at 9-14 mph.   (io) $12.7°C$.
(11) Small scattered echoes sometimes compressed into larger echoes and moving from west to east.   (12) RW and R-* combined.
(13) RHI radar observations showed that the convective cell grew to a height of 10 km. Above 600 mb the wind direction coincided with the direction of the movement of the echoes; at lower levels the wind moved in the opposite direction. Although the convective cell was tall, N_D curves for the data were of the symmetric mono-modal type.   "

11/25/57

(1) 1242-1304.   (2) A = 470; b = 1.41.   (3) Cold front; the front extended to the southwest from a low which was developing over N. and S. Carolina.   (4) SW, at 17 mph.   (5) A trough below the 300 mb level over the Midwest.   (6) SW, at 55-60 mph

at 200 mb.   (7) Type III.   (8a) 930 and 750 mb.
(8b) 3.0°C.; 4.6°C.   (9) SW, at 15-20 mph.   (10) 22°C.
(maximum: 27.0°C. at 650 mb).   (11) A line of small echoes,
oriented NE-SW in one string; each echo moved from SW.   (12) RW.
(13) N_D curves covered a wide spectrum, but with relatively low
concentration. Some column echoes reached 12 km and exhibited
shear in their tops. In such convective cells strong updrafts
would have existed. Large S values of the coalescence process
should be expected arid probably caused the wide spectrum of the
N_D curves. As item (9) in this summary indicates, the environ-
mental air was very dry. The relatively low concentration of
drops might have been due to mixing with dry air and to evapora-
tion of the isolated convective cloud. The consequent strong
updraft and evaporation caused the A value to become very large.
The effect of evaporation on the A value is explained by the
results calculated by Atlas and Chmela[1] and by Imai.[2]

11/27/57**

12/23/57

(1) 0900-0917; 1250-1420.   (2) A = 309; b = 1.30.   (3) Over-
running on the southern edge of a high which covered the east coast
of the United States; a well developed deep cyclone in central
Canada.   (4) ENE-E, at 21-25 mph.   (5) ENE surface wind backed
with increasing altitude to WNW, at 200 mb.   (6) None. . (7)
Type II.   (8a) 930 mb.   (8b) 1.9°C.; 2.1°C.   (9) WNW, 21-25
mph.   (10) 19.2°C.   (11) Scattered echoes very similar to
those for 11/27/57, except that many of them had slightly diffused
echoes and the direction was SE-E.   (12) TRW-.   (13) The
synoptic situation was very similar to that for 11/27/57. However,
the stable layer near 600 mb became weak; the instability aloft
also increased in the evening and caused TRW to develop. The
sounding indicated that instability energy was not as high as it
was in most other cases of TRW and that the environmental air was
quite arid in the morning. In such a case dN/dR, as noted in

**See page 46 for the case of 11/27/57.

Section 4.f., can be relatively high because precipitable drops
would decrease in size by evaporation from mixing with dry air
when the updraft is not powerfully supplied. This case was inter-
mediate between TRW and RW„

12/26/57

(1) 1151-1156; l629-1709. (2) A = 550; b = 1.165.   (3) Pre-
cold frontal; the front extended from a large depression over
Hudson Bay, Canada, to the Gulf of Mexico. The trough of the cold
front moved very rapidly to the east.   (4) SE-SSE, at 15-20 mph.
(5) A trough from the surface to south over the Midwest; winds
generally WSW above 500 mb over the south.   (6) 55-66 mph, at
300 mb-250 mb.   (7) Type II.   (8a) 930 mb.   (8b) 3.0°C;
3.0°C.   (9) W, at 21-25 mph.   (10) 15.5°C. at 550 mb.
(11) A line echo composed of small solid echoes (cold frontal echo)
and a diffused rainband composed of superimposed echoes (pre-cold
frontal echo).   (12) TRW; the pre-cold frontal rain was weak
and there was nearly continuous type rain; thunder was heard during
the shower when the cold front passed the station.   (13) Only
six minutes of raindrop data were taken during the pre-cold frontal
squall line; 26 minutes of data were taken during the cold frontal
rain. The large A value also implied a strong forced updraft. The
environmental air was dry and instability was not high.

1/2/58

(1) 1505-1603.   (2) A = 187; b = 1.39.   (3) Overrunning;
high pressure developed over the central and southwestern United
States (Miami was on the southeast edge of the system); a cyclone
was beginning to develop on the front near Cuba.   (4) NNE, at
21-25 mph.   (5) Miami was to the southeast of the large trough
which extended from Canada to Mexico.   (6) SW, at 71-77 mph,

from 400 mb-250 mb.   (7) Type VII.   (8a) No LFC.
(8b) -1.0°C.; -1.0°C.   (9) SW, at 55-60 mph.   (10) 1.2°C.
(11) Stratified and diffused echo developed over an extended area;
small elemental echoes moved to the northeast.   (12) R*.
(13) R* fell from the cloud layer above 800 mb. N_D curves had
narrow spectra in spite of the fact that the modes for the curves
were quite large. More nearly solid echoes appeared in the south-
west part of the echo mass; they soon stratified as they moved to
the northeast. The velocity of the echoes increased. The dif-
fused echoes showed the ice phase growth of precipitation particle
established. The narrow spectra (width 1 mm) of drops may be due
to sublimation growth; the relatively large mode diameter (1.5 mm),
to accretion growth of cloud droplets.

                           1/3/58

(1) 1148-1254.   (2) A = 445; b = 1.31.   (3) Warm frontal
rainfall was observed just behind the wave crest of the low.
(4) N, at 21-25 mph.   (5) The axis of the trough passed the
station at 700 mb sometime during the day.   (6) SW, at 55-77
mph from 500 mb-400 mb and SW, up to 83 mph at 250 mb-200 mb.
(7) Type VI; however, Type VII was recorded at other stations
around Miami.   (8a) 910 mb; the top of the convection was
750 mb; 750 mb-600 mb was a very stable dry layer. (8b) -8.8°C.;
-9.5°C.   (9) SW, at 96-100 mph between 500 mb and 800 mb;
NE at 22 mph between 700 mb and the surface.   (10) 20°C.
(11) Stratified by grainy echo extended in plan (no REE obser-
vations). The grainy element moved to the northeast, thus coin-
ciding with the direction of the winds from 400 mb to 300 mb.
(12) R*.   (13) Small echo elements moved ENE or NE. The
sounding indicated that the cloud layer was below 750 mb; a very
dry layer developed above 750 mb. Wet bulb temperatures had a
tendency to come close to the ascending curve at 400 mb, though
the; humidity sounding did not extend to this height. Data from

the soundings and echo movement suggest the following conditions
as the most likely explanation of the precipitation mechanism:
Snow particles from the precipitating cloud (350 mb, -31°C.)
after falling through the dry layer, grew by accretion when they
reached the nonprecipitating cloud (750 mb, 1.0°C.). The N_D
curves observed had relatively large A (445); this relatively
large median diameter for the N_D curves would be caused by evapo-
ration through 6 km in the ice phase and by accretion in the lower
cloud. The N_D curves were quasi-symmetric and monomodal and had
relatively large mode sizes.

                            1/7/58

 (1) 0038-0141.   (2) A = 343; b = 1.67.   (3) Occluded fronts
an occluded low, moving to the northeast, passed Florida. The
storm observed occurred within the cold sector between an occluded
crest front and cold type occluded front. The low deepened
rapidly.   (4) WSW, at 12-20 mph.   (5) A trough (surface to
150 mb) extended from Canada to Texas.   (6) No data.
 (7) Type VI; a station 17 miles south and another 12 miles west of
Miami observed Type II or Type III. .   (8a) No LFC.   (8b) 0.0°C;
-1.0°C.   (9) No data.   (10) 3.2°C. at 500 mb.   (11) Broad
and stratified rainband; small echo elements moved from SW to NE
at 63 mph.   (12) R*.   (13) R was very low at the camera
station as compared with R for nearby stations. The generating
cloud layer was estimated to have been at 500 mb-400 mb (-10°C.
to -22°C.). The N_D curves had large drops when R increased
 (though R was still quite low). The data for winds aloft were
missing, but it is reasonable to assume that sorting took place;
the large b value is probably a result of the sorting effect. The
clockwise cycles of the chronological Z-R trace indicates the
sorting effect.

1/21/58

(1) 1648-1743.   (2) A = 300; b = 1.50.   (3) Pre-cold frontal: an occluded low developed over the Midwest and moved to the northeast. The cold front extended from this low passed Miami at 0000 on 1/22/58.   (4) ESE, at 15-20 mph.   (5) Eastern edge of a deep trough; SW winds developed over Florida.   (6) 55-60 mph at 400 mb; no data for higher levels.   (7) Type VII. (8a) No LFC. (8b) 0.0°C.; -4.5°C.   (9) W, at 9-14 mph. (10) 5.5°C. (11) Stratified broad band; small echo elements moved to ENE.   (12) R*.   (13) The N_D curves have relatively broad spectra. The curves suggest that coalescence growth predominated. The sounding and echo movement indicated that the cloud layer in which precipitation began was above 700 mb — probably around 600 mb (0.0°C.). The cloud top appeared to have been above 300 mb. Wind shear between 500 mb and 700 mb was very slights difference between wind velocity for the two levels was 5 mph. It might be concluded that efficient coalescence occurred through the melting layer between well developed and high concentration snow flakes, since, if most of the dendritic, they coalesce rapidly in the melting layer.

1/23/58

(1) 1640-1643.   (2) A = 591; b = 1.04.   (3) Warm frontal; a low approached from southern Texas; the warm front extended to the east; south of Miami.   (4) E, at 9-14 mph.   (5) A large deep trough developed from northern Canada to Mexico throughout the entire troposphere.   (6) As high as 90 mph, at 500 mb-150 mb.   (7) No appreciable amount recorded; the following stations recorded Type VII: Tamiami (7 miles NW of camera station), International Airport (6 miles NNE), and Hialeah (8 miles N).   (8a) No LPC. (8b) -3.5°C.; -6.0°C.   (9) WSW, at 44-49 mph.   (10) 9.0°C. (minimum, 1.0°C. at 570 mb).   (11) Diffused

stratified and scattered echo elements moved to the N or N-NW;
however, some of the southern echoes moved to the NE.   (12) R*.
 (13) Though only four Z-R points were available, the N_D curves
shown in Figure 8 are a representative case of small b, large A.
The points are located almost on a straight line. The rain ob-
served was from a cloud below 800 mb.

2/7/58

(1) 08,45-0910; 1013-1111.   (2) A = 392; b = 1.31 and 2.0.
 (3) Pre-cold frontal squall line TRW; however, the data were
collected in the preceding light RW and in the extended R which
followed the TRW.   (4) S, at 9-14 mph.   (5) Eastern edge
of a trough which extended through the entire troposphere. A
strong WSW wind prevailed over the southeastern United States.
 (6) SW, at more than 100 mph (taken from adjacent surroundings).
 (7) Type V for RW and R; Type II for TRW.   (8a) 925 mb.
 (8b) 5.3°C.; -1.0°C.   (9) No data.   (10) 4.0°C.
 (11) Plane type stratified echo, diffused in the back, solid in
the front, echo element moved to the E and NE.   (12) TRW (see
Item 3).   (13) Only ten minutes of data were collected in the
RW; 58 minutes were collected in the R* which followed the TRW.
The large b values which was obtained during the R* may have been
a result of the sorting effect during the fall of the drops from
a stratified cloud which was estimated to have been above 500 mb.

3/19/58

(1) 0747-0750; 0837-0841; 0907-1026. (2) A = 374; b = 1.89.
 (3) Pre-cold frontal; a cold front from a cyclone off the coast
of Massachusetts across the Florida peninsula.   (4) S, at 9-11
mph.   (5) A trough extended from Canada to the Gulf of Mexico
at 700 mb; there was a southwest wind field over the Midwest and
Southeast.   (6) SW, at 67-71 mph, at 700 mb.   (7) Type VI.

(8a) 680 mb (positive convective energy was slight).   (8b) 0.5°c.;
-1.0°C.   (9) SW, at 61-66 mph (700 mb - 1000 mb).   (10) 1.2°C.
(11) Stratified echoes in a broad band.   (12) R*.   (13) The
generating clouds were not thick; precipitation was rather weak.
Other raingage stations around Miami also indicated weak rain.
The most noticeable effect of the weather situation on the N_n
curves was thought to be the sorting effect, since the clouds
were above 700 mb and strong wind shear occurred below this level.

3/24/58

(1) 1446-1556.   (2) A = 230j b = 1.60.   (3) Pre-cold frontal;
a wave cyclone moved to the west in Alabama.   (4) SE, at 21-25
mph.   (5) A low was indicated around southern Illinois below
300 mb; a wind, generally SE, over Florida.   (6) W, at 55-66
mph, at 200 mb.   (7) Type I.   (6a) 790 mb.   (8b) 3.0°C;
0.4°C.   (9) WNW, at 38-43.   (10) 12°C.   (11) Diffused
and stratified rain band extended NE-SW.   (12) TRW.
(13) N_D curves changed by mode shift R =10 mm/hr; then smaller
drops (about 2 mm) and the group of drops larger than 3 mm over-
lapped each other and made a composite N_D curves (as described in
Section 2.e. using data from two other days). Thus, the consid-
ably larger b value was obtained. A small cell which formed at
the edge of the extensive TRW echo area moved to the interior
portion of the TRW echo; the raingage trace showed this feature.
The Z-R points can be subdivided into three regression lines;
initial (large b value), mature (medium b value), and final (small
b value) stages. Z-R plots had no clockwise cycle in the mature
stage (plots for the initial stage did have them); the mature stage
is shown as a completely amalgamated echo on the PPI scope.

4/11/58

(1) 1140-1314.   (2) A = 312; b = 1.39.   (3) Pre-cold frontal;
a wave cyclone developed over Maine; a cold front passed over the

Florida peninsula.   (4) SW, at 9-14 mph; after the front passed, N-NW, at 5-8 mph.   (5) WSW, in front of a broad trough at 700 mb-150 mb.   (6) SW-WSW, at more than *67* mph, above 500 mb, (7) Type IV.   (8a) 925 mb.   (8b) -7.3°C; -5.0°C.   (9) WSW, at 44-49 mph.   (10) 15°C.   (11) Small blocks of echoes composed of solid convective echoes; each elementary convective echo moved to NE or ENE at an average speed of 45 mph.   (12) TRW (thunder heard to the southwest during a short shower). (13) The sounding indicated a large positive area of instability. Each convective echo block was comparatively small, and a single drop trace was drawn by the raingage. Three peaks of rain were observed for the cell which passed the station, all of which formed the single block of echo. That no clockwise cycle of the Z-R plots was evident for this case accords with the description in Section l.c.

<center>4/15/58</center>

(1) 1622-1629.   (2) A = 246; b = 1.46.   (3) Pre-cold frontal; a wave cyclone centered in Alabama had a warm sector which covered Florida at 1500.   (4) SW, at 15-20 mph. (5) On the 700-mb map a low was apparent over Illinois and Missouri below 300 mb at 0600; winds aloft above 700 mb.   (6) None.   (7) Type v. (8a). 940 mb.   (8b) 5.2°C.; 6.0°C.   (9) WNW, at 26-31 mph, (10) 5.5°C.   (11) Plane and line echoes composed of a number of small solid echoes; all echoes moved to the east,   (12) RW, (13) Although convective instability was observed, TRW activity did not develop. Data were collected only for seven minutes,

<center>5/5/58</center>

(1) 0905-0933; 1219-1241.   (2) A = 417; b = 1,29.   (3.) Easterly wave and pre-cold frontal combined,   (4) 3E, at 9-20 mph, (5) SE wind, at 15-25 mph, caused by a subtropical high, prevailed

below 400 mb.   (6) 61-66 mph, at 200 mb.   (7) Type I; ad-jacent stations recorded Type II.   (8a) 910 mb (at 0700 and 1900).   (8b) 6.9°C; 8.3°C. (at 0700 and 1900).   (9) E, at 5-8 mph.   (10) 6.3°C.   (11) Small block echoes, linked with adjacent echoes, moved to the southeast at 27 mph; the direction coincided with the wind shear between 300 mb and 400 mb. (12) TRW.   (13) The Z-R points were divided into two groups: forenoon and afternoon. Both were TRW. The easterly wave deepened in the afternoon. The A values were smaller for the forenoon storm. The only clockwise cycle among the Z-R plots occurred in the afternoon storm — additional evidence for the conclusion mentioned in Section l.c.

5/6/58

(1) 0857-0956.   (2) A = 345; b = 1.56.   (3) Pre-cold frontal; one cyclone wave moved to the northeast across all the southeastern states except Florida (0900).   (4) SE-SW, at 5-14 mph.   (5) A trough, extending from Canada to the Gulf of Mexico, appeared below 150 mb at 0600.   (6) Above 300 mb; maximum was 78-83 mph at 200 mb.   (7) Type I (and Type IV).   (8a) 940 mb.   (8b) 7.2°C; 10.0°C.   (9) WSW, at 21-25 mph.   (10) 10.1°C. (11) No radar observations.   (12) TRW.   (13) Raindrop data were collected for 11 minutes at the beginning of the storm. The steep slope of the raingage trace implied high R and Z values; however, data were not collected for the time which the raingage trace had the highest R. It is reasonable to assume that inclusion of data for this time would result in higher A values. This storm Is a case of large positive area of instability as shown in item (7) above.

5/13/58

(1) 1415-1451.   (2) A = 628; b = 1.25.   (3) Trough aloft.
The surface map at 0900 showed wave cyclones over Montana and Nova
Scotia. . A front from the two lows passed through South Carolina,
Georgia, and Alabama on the southern edge of the associated high.
pressure area which occupied the Midwest.   (4) Between N and E,
at 1-4 mph.   (5) A relatively sharp trough (from northeast
Canada to the northern neck of the Florida peninsula) occurred
on maps for all levels from 700 mb to 150 mb.   (6) None.
(7) Type II.   (8a) 880 mb.   (8b) 6.3°C; 4.0°C.   (9) WSW,
at 26-31 mph.   (10) 3.3°C.   (11) A large TRW echo, which
was composed of quite small amalgamated echoes, passed the station.
The small echo elements moved to the E and E-SE near the center of
the large TRW echo.   (12) TRW.   (13) The aerological situa-
tion was the typical TRW case; the heaviest observed instantaneous
R for a one-minute sample in this TRW was 721 mm/hr; there were
4781 drops per cubic meter. The high concentration of drops and
the large A value for this case are typical characteristics of
Miami rainfall as noted by Mueller and Jones.[4] The large positive
area of instability indicated strong updraft; relatively high
liquid water content observed at the surface and entrainment of
air with the high mixing ratio indicated that there was high
liquid water content in the cloud.

5/23/58

(1) 1022-1120.   (2) A = 251; b = 1.30.   (3) Easterly wave;
a high pressure cell over the northern Midwest; a weak ridge of
subtropical high pressure over the South; a weak low over the
northwestern Caribbean.   (4) E-NE, at 5-14 mph.   (5) High
pressure existed at all altitudes up to 15 mb over the Carribbean.
(6) There was high pressure aloft at 700 mb over the Atlantic,
northeast of Cuba. This high appeared over the eastern Caribbean

at 150 mb. Wind aloft at Miami was southerly below 500 mb.
 (7) Type III (and Type VII); the raingage trace was Type III at
first, but it gradually became Type VII. The raindrop data were
taken during the Type III trace.   (8a) 920 mb.   (8b) 4.0°C.;
5.2°C.   (9) SW, at 21-25 mph.   (10) 1.4°C.   (11) The
plane type stratified echo combined a number of small and scattered
echoes. Echo elements moved to the northwest at 14 mph.
{12) RW and R*.   (13) N_D curves for this storm were of the sym-
metric monomodal type. The fitting curve (Eq. 6) shows that the
N_D plots fit quite well to the random coalescence equation, where
s = 3. This storm is also a typical case for small A and small b
values. The symmetric monomodal N_D curve changes its peak height
without shifting its mode appreciably when R increases. Since the
environmental air was quite humid below 300 mb, the N_D curves would
not have been affected by evaporation even at the edge of the pre-
cipitation cloud. A mode shift often occurred, even when the N_D
curves remained symmetric and monomodal, whenever the Z-R point
fell a considerable distance from the other Z-R points which de-
termined the regression line. This was probably caused by the
differences between S (coalescence factor) and CH (accretion
growth) for edge and middle of the bubble of the updraft. In
this case, the small A could be caused by evaporation.

                        5/24/58

 (1) 1243-1300.   (2) A = 123; b = 1.59.   (3) Easterly waves;
high pressure over Quebec, Canada. The slowly developing low over
Cuba moved to the east.   (4) SE-E, at 15-20 mph.   (5) There
was a deep low at 500 mb over northern Canada from which a trough
extended to the south. A small low appeared at all levels over
southeastern Texas. The wind aloft was southerly below 400 mb
in the morning; in the evening the wind was northeasterly below
800 mb and southerly between 800 mb and 400 mb.   (6) None.
 (7) Type VII.   (8a) 750 mb.   (8b) 0.50°C.; 1.0°C.

(9) Unknown; probably weaker than 20 mph.   (10) 22.7°C. at 0700;
8.5°C. at 1900 (5.0°C. at 520 mb).   (11) Broad rainband and
stratified plane echo.   (12) R*.   (13) The rain was caused
by the small low which passed just south of Key West, Florida.
The morning sounding at Miami showed the upper air to have been
quite dry; however, continuous rain was recorded at that time.
The sounding taken in the evening gave a more acceptable indica-
tion of the humidity. The Z-R regression line for this case showed
small A, large b values. N_D curves for extremely high, scattered
Z points on the Z-R plots were nearly symmetric and monomodal.
The few drops larger than 5 mm which caused the high Z points
were also responsible for the deviation from symmetry at the higher
end of the curve. Since the spectra were evidently broken between
two modes, it is difficult to believe that the large drops and the
great number of small drops were caused by the same mechanism.
The largest drop size diameter measured for this storm was 7.1 mm.

7/25/58

(1) 1605-1640.   (2) A = 426; b = 1.67.   (3) Easterly wave;
the western edge of the Azores high covered Florida and the eastern
half of the Gulf of Mexico.   (4) Calm.   (5) Very flat pres-
sure gradient below 150 mb over Florida and the Caribbean area.
(6) None.   (7) Type I.   (8a) 860 mb.   (8b) 5.2°C.; 5.6°C.
(9) SW, at 15-20 mph.   (10) 7.5°C.   (11) Small scattered
spots and blocks which moved to the southeast at 12 mph; block
echoes of the TRW showed that they were assemblies of small echoes.
(12) TRW.   (13) This is a typical case of the isolated TRW cell.
Although the raingage trace was classified as Type I, it was quite
similar to Type IV. Because the radar was too close to the camera
location, it was not possible to determine which part of the TRW
cell passed the camera station. The extremely broad and low peak
spectra might have been an indication that the edge of the cell
passed the camera station.

11/27/57

(1) 0801-0854; 1406-1441.   (2) A = 339; b = 1.9.   (3) Air
mass showers on the southwestern side of a high pressure system
which covered Florida and Missouri; lows in Wisconsin and Texas.
 (4) E, at 9-14 mph.   (5) SE winds below 700 mb; SW winds above
700 mb.   (6) 55-66 mph at 200 mb-150 mb.   (7) Type III
 (and VII); rather close to TRW.   (8a) 900 mb and 440 mb.
 (8b) -1.0°C. and -0.2°C. at 0700; 0.2°C. and 3.5°C. at 1900.
 (9) W, at 26-31 mph.   (10) 22°C.   (11) Small grouped and
scattered cellular echoes most of which moved from SSW-SW. The
direction coincided with that of the wind below the inversion
layer at 550 mb.   (12) RW.   . (13) Most of the early showers
from which data were taken were warm type rains, though later, as
the instability was increased by cold advection, TRW developed.
N_D curves are symmetric and monomodal; A is relatively large,
while b is small. The small echoes moved at 12-10 knots.

REFERENCES

1. Atlas, David and A. C. Chmela, "Physical-Synoptic Variations
    of Raindrop Size Parameters," Proceedings of Sixth Weather
    Radar Conference, American Meteorological Society, pp. 21-29,
    1957.

2. Imai, Ichiro, "Raindrop Size Distributions and Z-R Relation-
    ships," Proceedings of the Eight Weather Radar Conference,,
    American Meteorological Society, pp. 211-215, 1960.

3. Marshall, J. S. and W. Palmer, "The Distribution of Raindrops
    with Size," Journal of Meteorology. Vol. 5, pp. 165-166, 1948.

4. Mueller, E. A. and D. M. A. Jones, "Drop-Size Distributions in
    Florida," Proceedings of the Eighth Weather Radar Conference,
    American Meteorological Society, pp. 299-305, 1960.

5. Blanchard, D. C., Observations on the Behavior of Water Drops
    at Terminal Velocity in Air, General Electric Laboratory
    Occasional Report No. 7, Contract 36-039-32427, Schenectady,
    New York, November, 1948.

6. Jones, D. M. A. and L. A. Dean, A Raindrop Camera, Research
    Report No. 3, Signal Corps Contract DA-36-039 SC-42446,
    Illinois State Water Survey, Urbana, Illinois, December, 1953.

7. Marshall, J. S., "Precipitation Trajectories and Patterns,"
    Journal of Meteorology, Vol. 10, pp. 25-29, 1953.

8. Imai, Ichiro, "Precipitation Streaks and Raindrop Size Distri-
    butions," Papers in Meteorology and Geophysics, Vol. 7, No. 2,
    pp. 107-123, 1956.

9. Jones, D. M. A., Rainfall Dropsize Distributions and Radar
    Reflectivity, Research Report No. 6, Signal Corps Contract
    No. DA-36-039 SC-64723, April, 1956.

10. Fujiwara, M. and Z. Yanayizana, A Note on Z-R Relations in
    Various Storms, a paper presented at the Annual Meeting of
    the Meteorological Society of Japan, 1956 (not printed).

11. Lamp, R., "Das Tropfenspektrum in Niederschlagen und die
    Radar Reflectivitat nach fremden und eigenen Messungen,"
    Beitrage zur Physik der freien Atmosphare, Vol. 30,
    pp. 223-245,   1958.   ~

12. Jones, D. M. A., and E. A. Mueller, "Z-R Relationships from
    Drop Size Data," Proceedings of the Eighth Weather Radar Con-
    ference, American Meteorological Society, pp. 498-504, 1960.

13. Blanchard, D. C, "Raindrop Size Distribution in the Hawaiian Islands," _Journal of Meteorology_, Vol. 10, pp. 457-473, 1953.

14. Best, A. C, "The Size Distribution of Raindrops," _Quarterly Journal of the Royal Meteorological Society_, Vol. 76, pp. 16-36, 1950.

15. Melzak, Z. A. and W. Hitschfeld, _Mathematical Treatment of Random Coalescence_, McGill University Scientific Report MW-3, Contract No. AP 19(122)-217, 1953.

16. Tsuji, M., Coagulation of Colloid Particles," _Memoirs of the Faculty of Science_, Kyushu University, Series, B, No. 1, pp. 74-79, 1953.

17. Diem, M., "Messungen der Grosse von Wolken elementen II," _Meteorologische Rundschau_, Vol. 1, pp. 261-273, 1948,

18. Weickmann, H. K., and H. J. Aufm Kampe, "Physical Properties of Cumulus Clouds," _Journal of Meteorology_, Vol. 7, pp. 404-405, 1953.

19. East, T. W. R., _Precipitation Mechanisms in Convective Clouds_, McGill University Scientific Report MW-22, Contract No. AF 19(122)-217, 1956.

20. Bowen, E. G., "The Formation of Rain by Coalescence," _Australian Journal of Scientific Research_, Series A, Vol. 3, pp. 193-212, 1950.

21. Ludlam, F. H., "The Production of Showers by the Coalescence of Cloud Droplets," _Quarterly Journal of the Royal Meteorological Society_, Vol. 77, pp. 402-417, 1951.

22. Howell, W. E., "The Growth of Cloud Drops in Uniformly Cooled Air," _Journal of Meteorology_, Vol. 6, pp. 134-139, 1949.

23. Neiburger, M. and C. W. Chien, "Computations of the Growth of Cloud Drops by Condensation Using an Electronic Digital Computer," _Physics of Precipitation_, Geophysical Monograph No. 5, pp. 191-209, 1960.
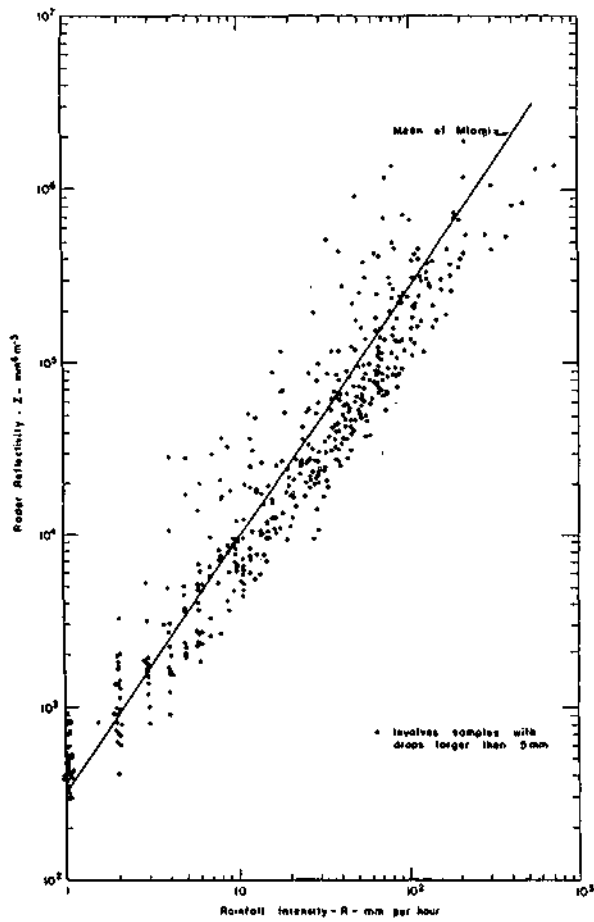
FIG. la Z-R PLOTS FOR 14 THUNDERSTORMS OBSERVED FROM 1957 TO 1958 AT **MIAMI**, FLORIDA
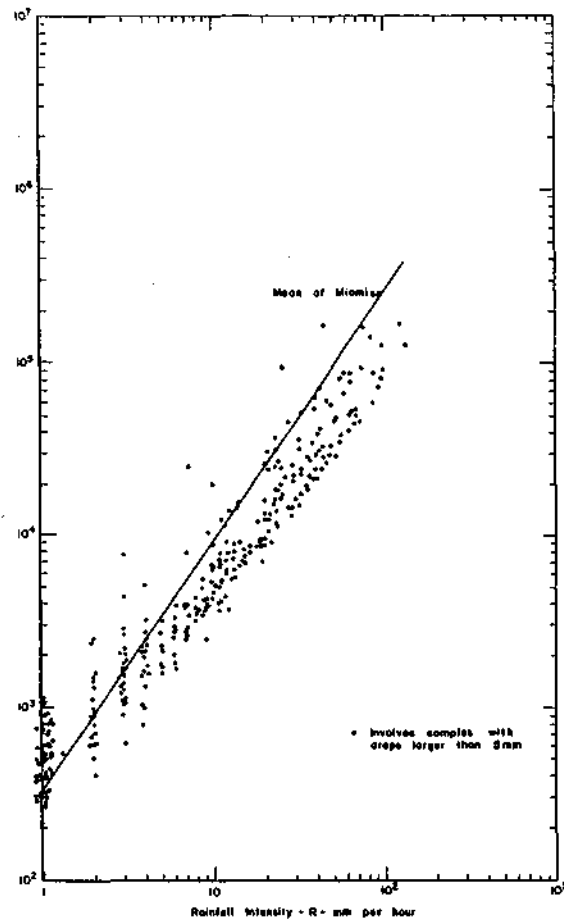
FIG. lb Z-R PLOTS **FOR 9** RAINSHOWER **STORMS OBSERVED FROM 1957 TO 1958 AT MIAMI, FLORIDA**
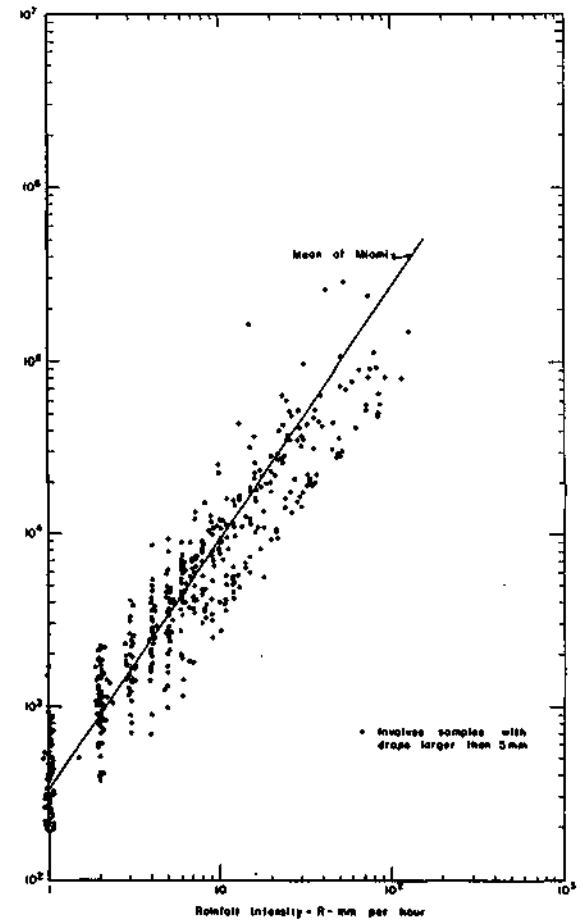
FIG. lc **Z-R PLOTS FOR 12 RAINSTORMS OBSERVED FROM 1957 TO 1958 AT MIAMI, FLORIOA**

(R=1 mm/hr)

0   +0.2   +0.4 +0.6 +0.8 +1.0

-0.1   -0.2   -0.3   -0.4   -0.5
mm/hr

**TOTAL
35 Storms**

Number Of Cases

**TRW
14 Storms**

**RW
9 Storms**

**R*
12 Storms**

0   .05   .10   .20   .30

$$\overline{\sigma}_{R/\overline{Z}} = \left[\sum_{j}^{N}(\log_{10}R_j - N\log_{10}r_j)^{\frac{1}{2}}/N\right]$$
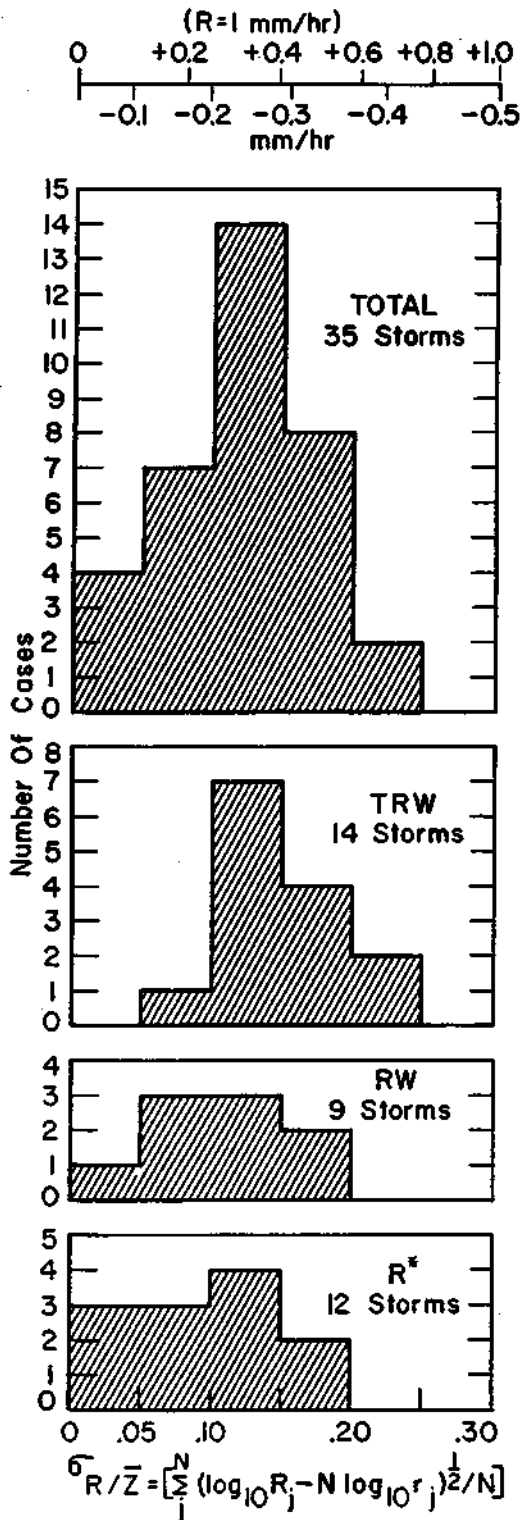
FIG.2 FREQUENCY OF STORMS WITH
THE STANDARD ERROR WHICH
MIGHT OCCUR USING Z - R
RELATION FOR MEASURING R
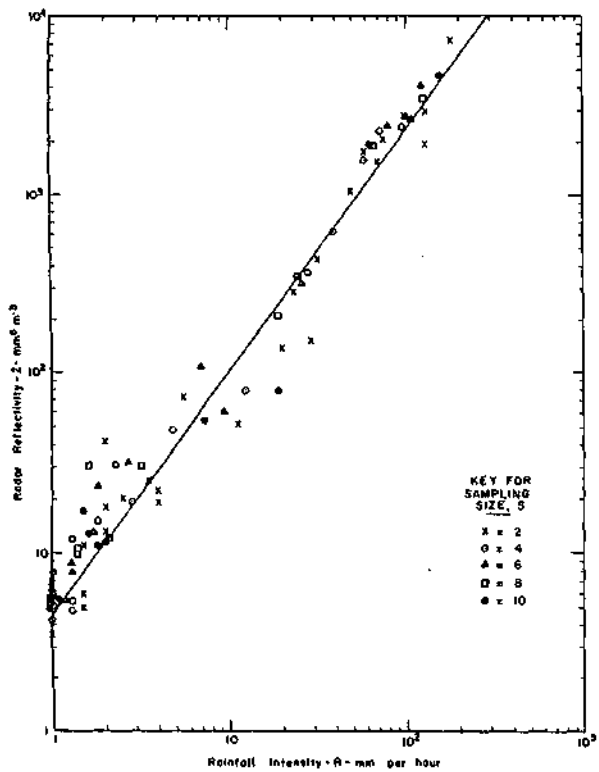
FIG. 3a SCATTER OF Z-R POINTS IN RELATION TO SIZE OF SAMPLE IN TRW OBSERVED 10/3/57 AT MIAMI, FLORIDA
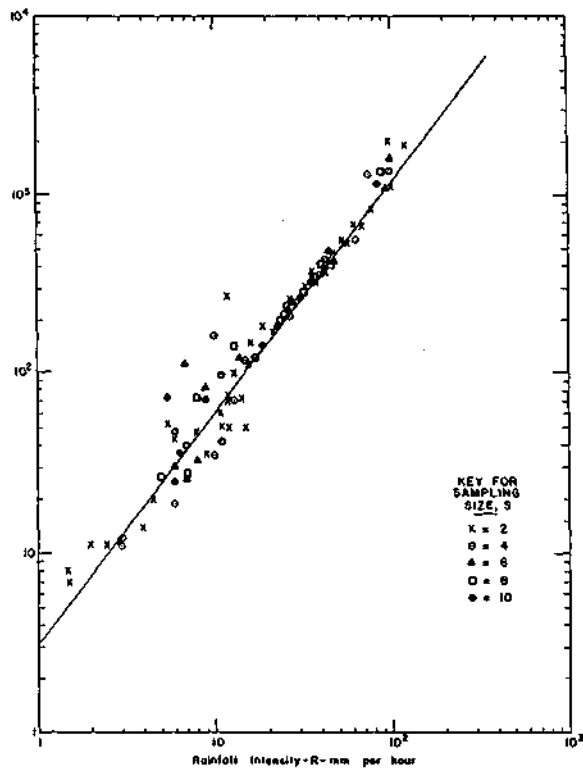
FIG. 3b SCATTER OF Z-R POINTS IN RELATION TO SIZE OF SAMPLE IN WEAK TRW AND RW OBSERVED 12/23/57 AT **MIAMI,** FLORIDA
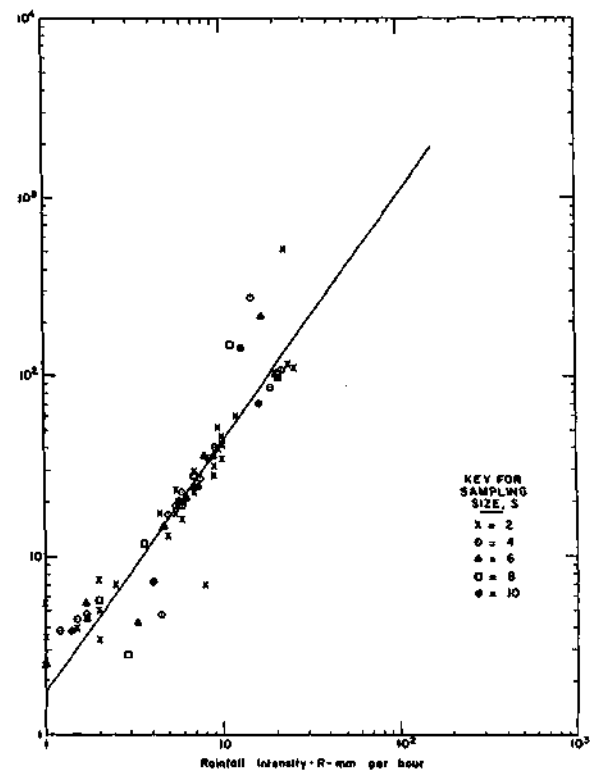
FIG. 3c SCATTER OF Z-R POINTS IN RELATION TO SIZE OF SAMPLE IN R^8 OBSERVED 1/2/58 AT MIAMI, **FLORIDA**
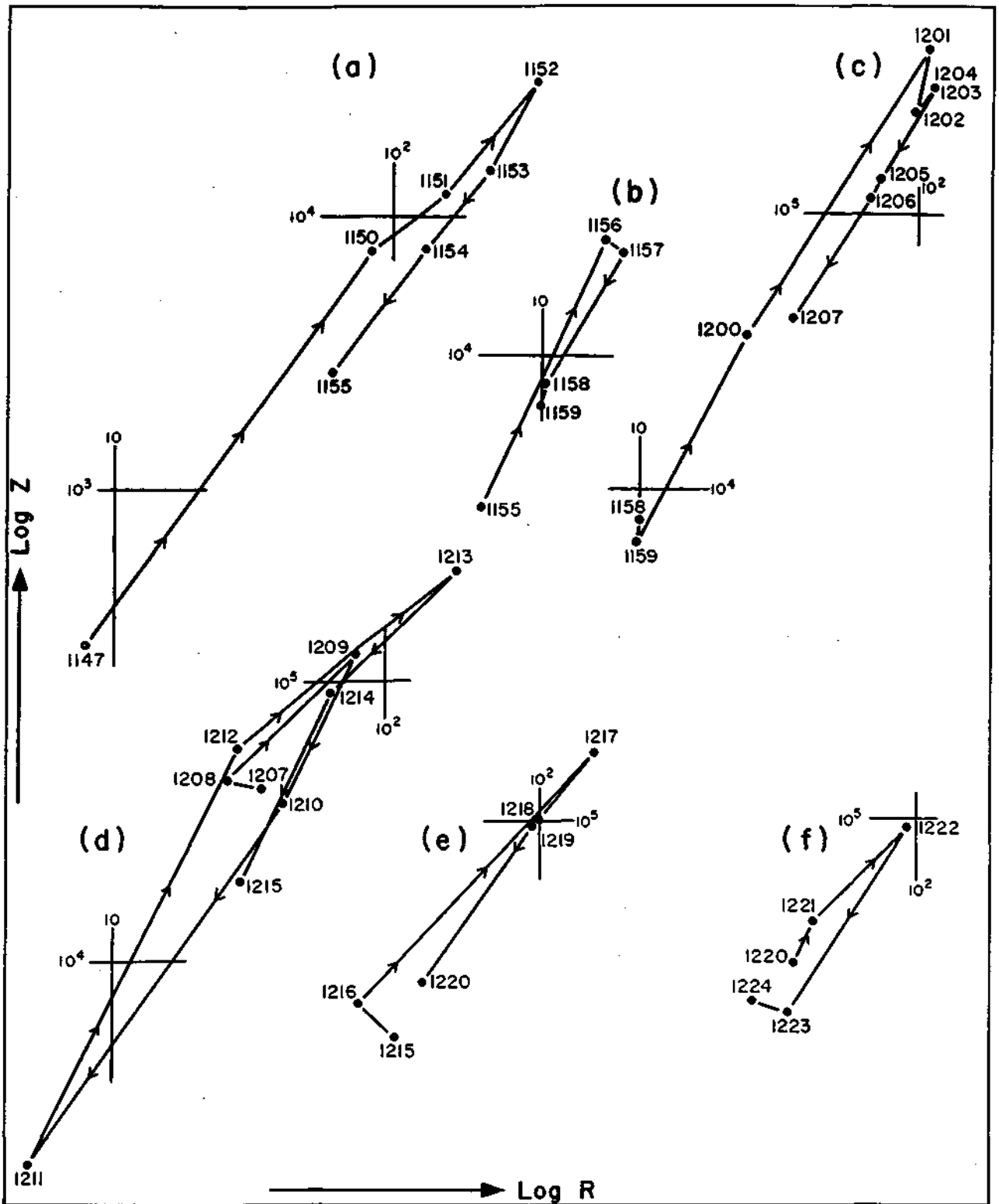
FIG. 4   CHRONOLOGICAL   CYCLIC   PATTERNS   OF   Z-R   RELATION
         REVEALED   IN   TRW   OBSERVED   8/28/57   AT   MIAMI, FLORIDA
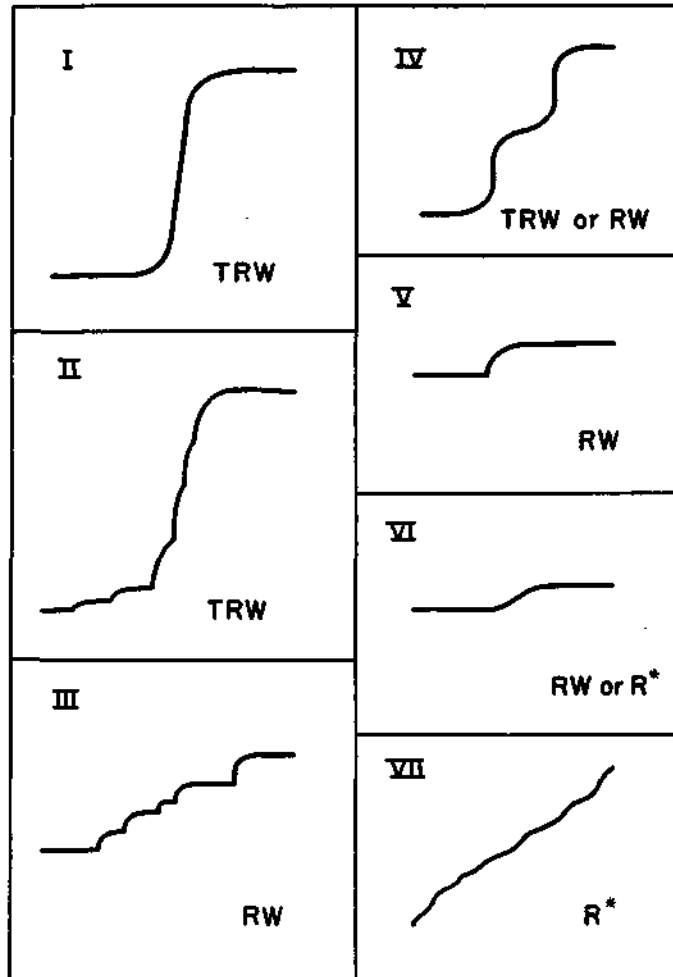
FIG. 5   CLASSIFICATION   OF   RAINGAGE TRACES
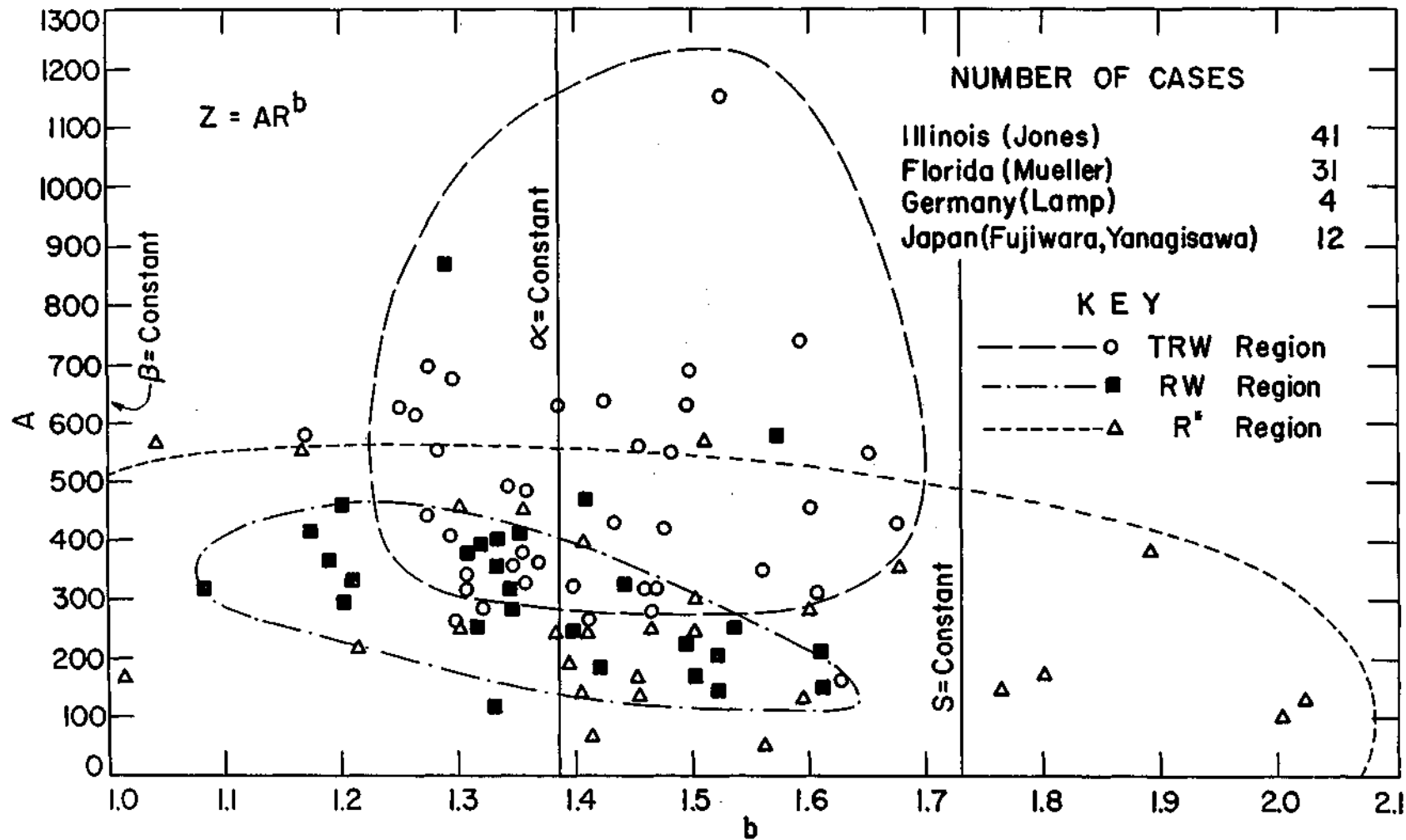
FIG. 6a PLOT OF A AND b FOR THREE TYPES OF RAINFALL
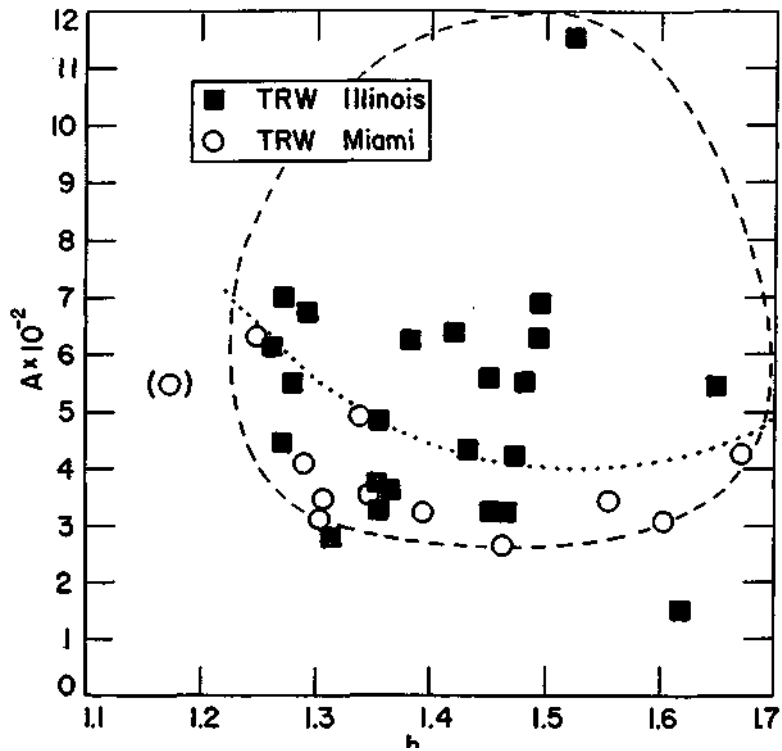
**FIG. 6b   PLOT OF A   AND b FOR THUNDERSTORMS
IN   ILLINOIS   AND   FLORIDA**
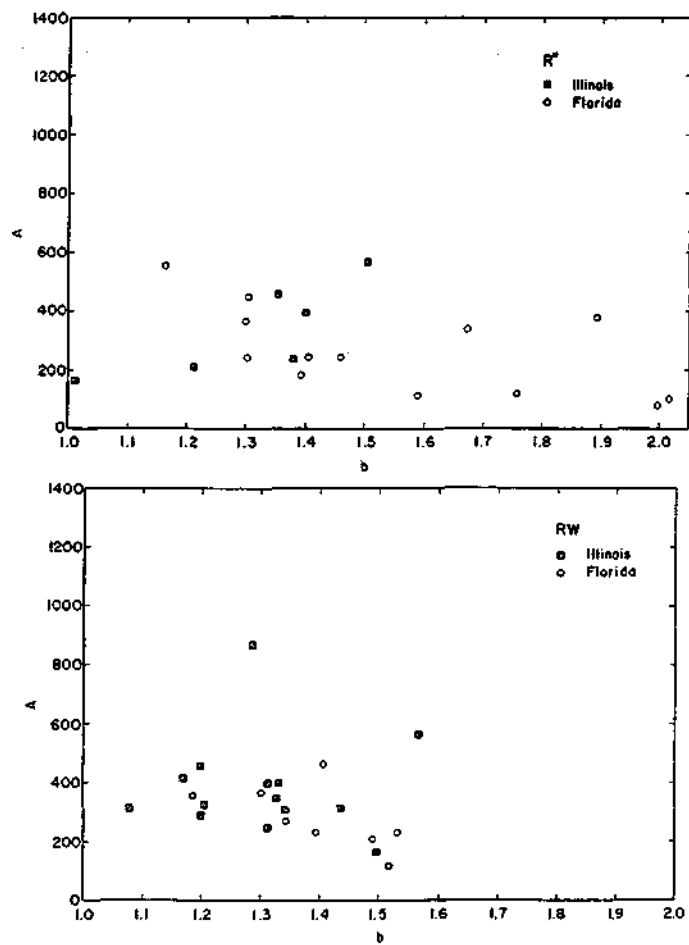
**FIG. 6c PLOT OF A AND b FOR RW AND R* IN
ILLINOIS AND FLORIDA**
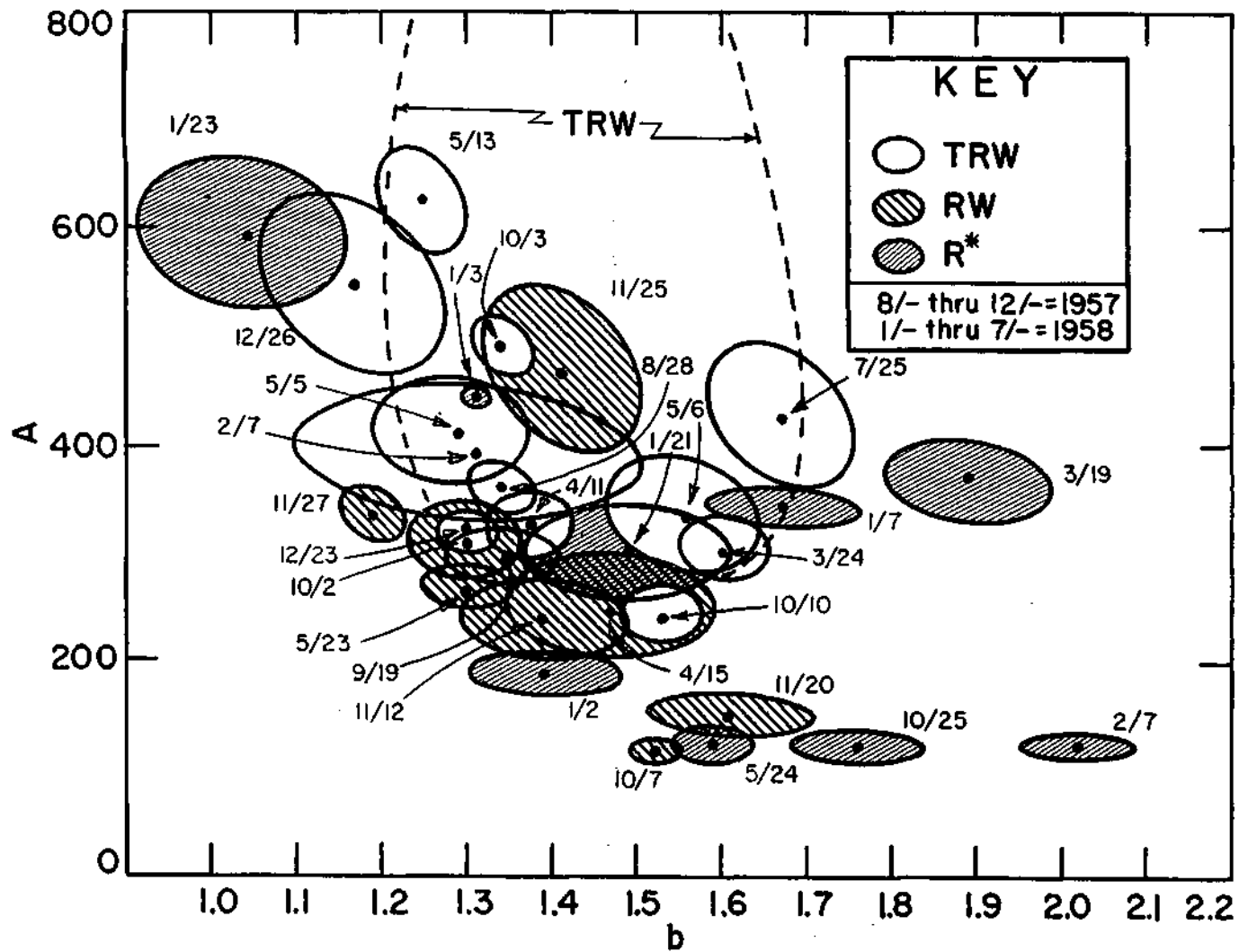
FIG.6d 95% RELIABILITY ELLIPSOIDS ON MIAMI DATA
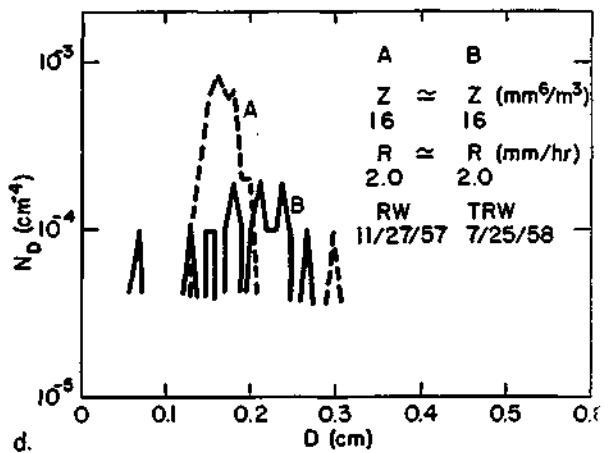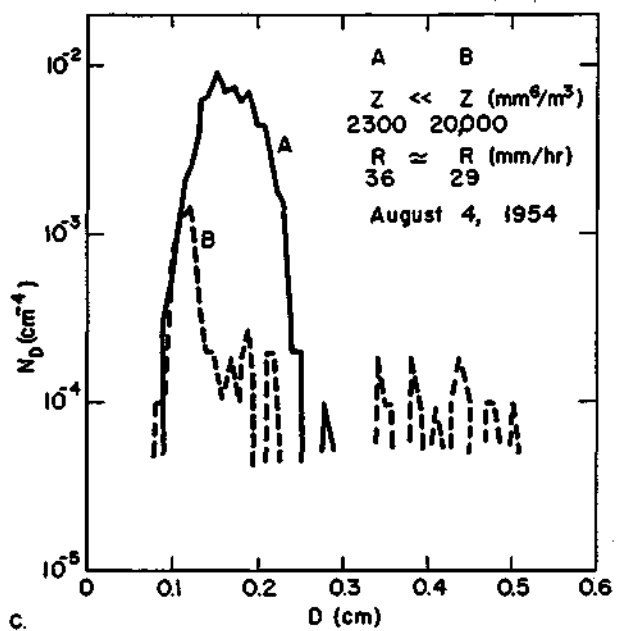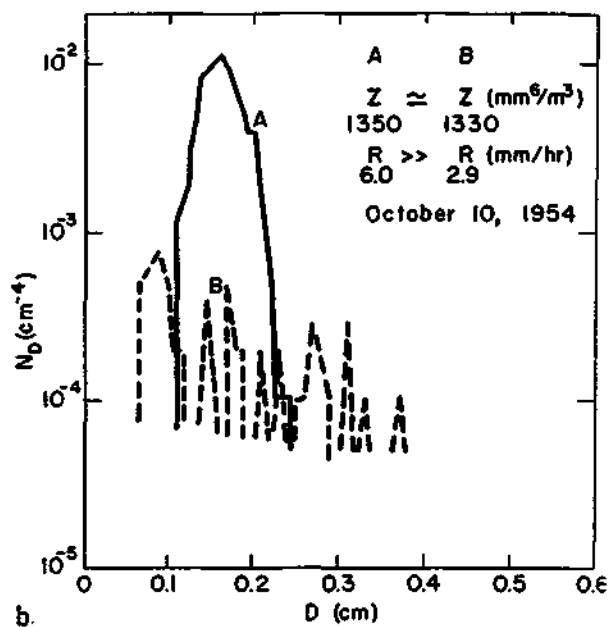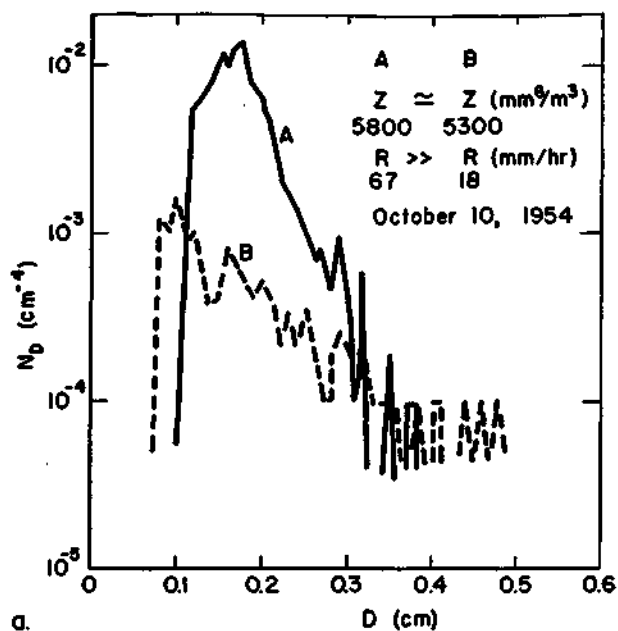
FIG.7a-d EXAMPLES OF N_D CURVES AROUND LOG Z-LOG R REGRESSION LINES
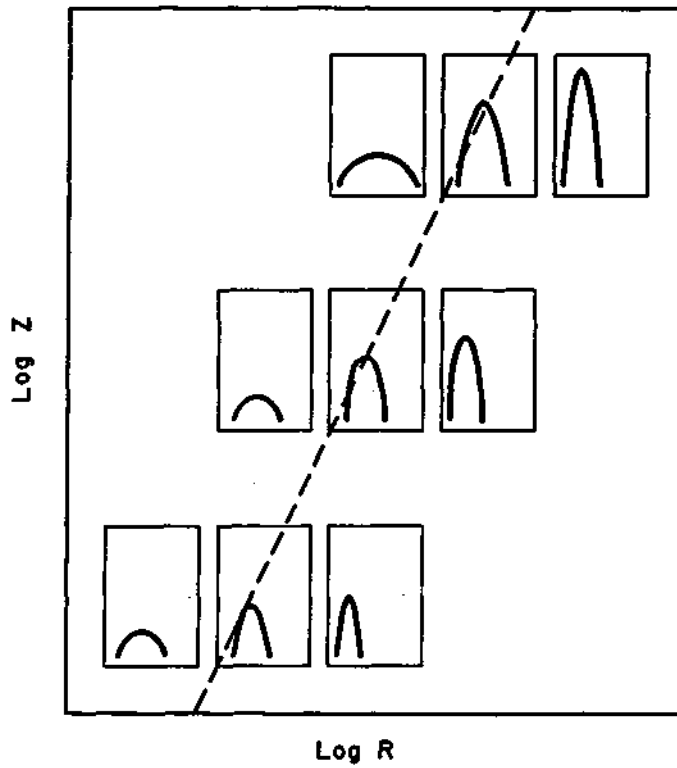
FIG. 7e A SCHEMATIC ILLUSTRATION
OF N_D CURVE CHARACTERISTICS
WITH RELATION TO THE LOCA-
TION OF Z-R POINTS
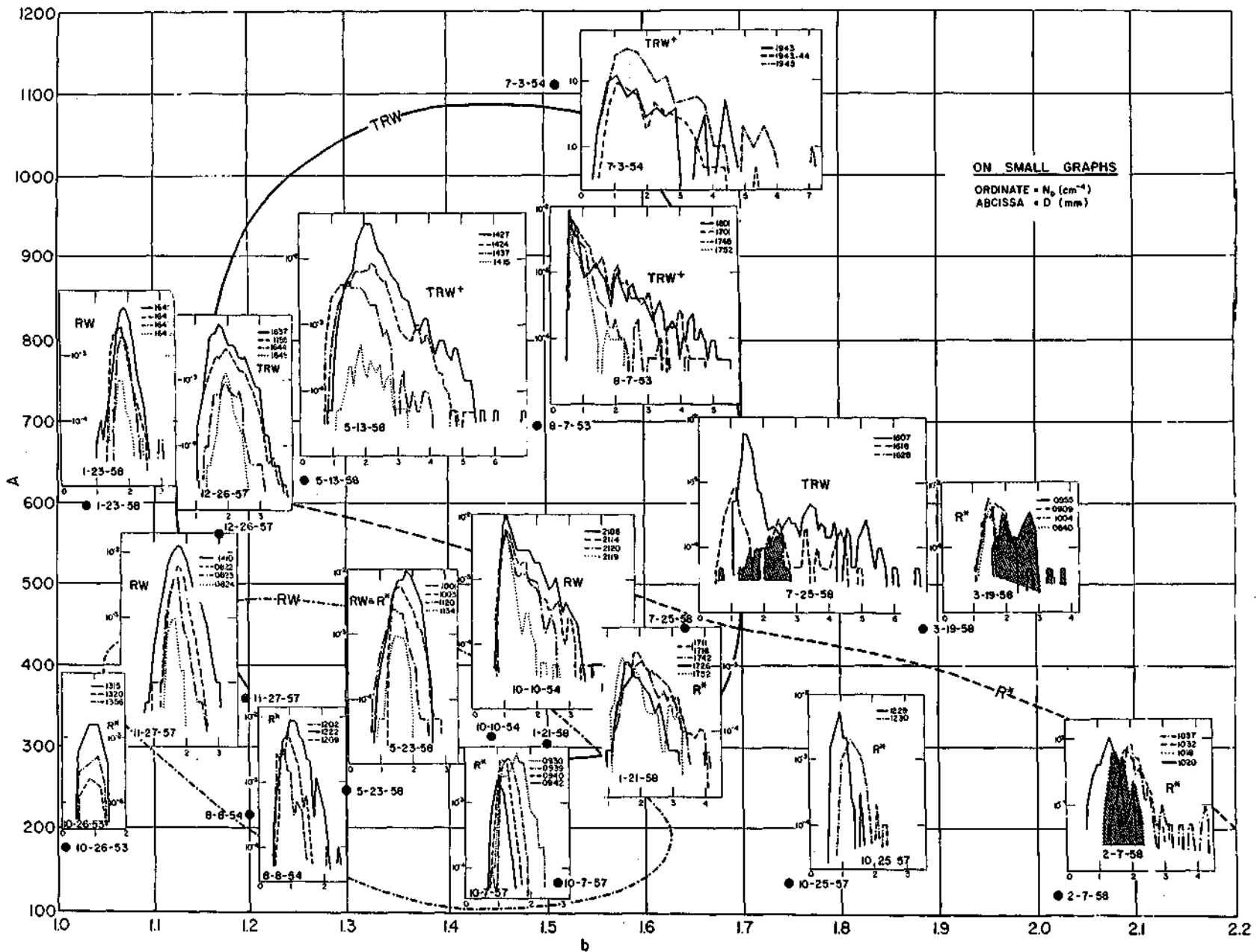
FIG.8   REPRESENTATIVE   TYPES   OF N_D - CURVES   ON   A, b   PLANE
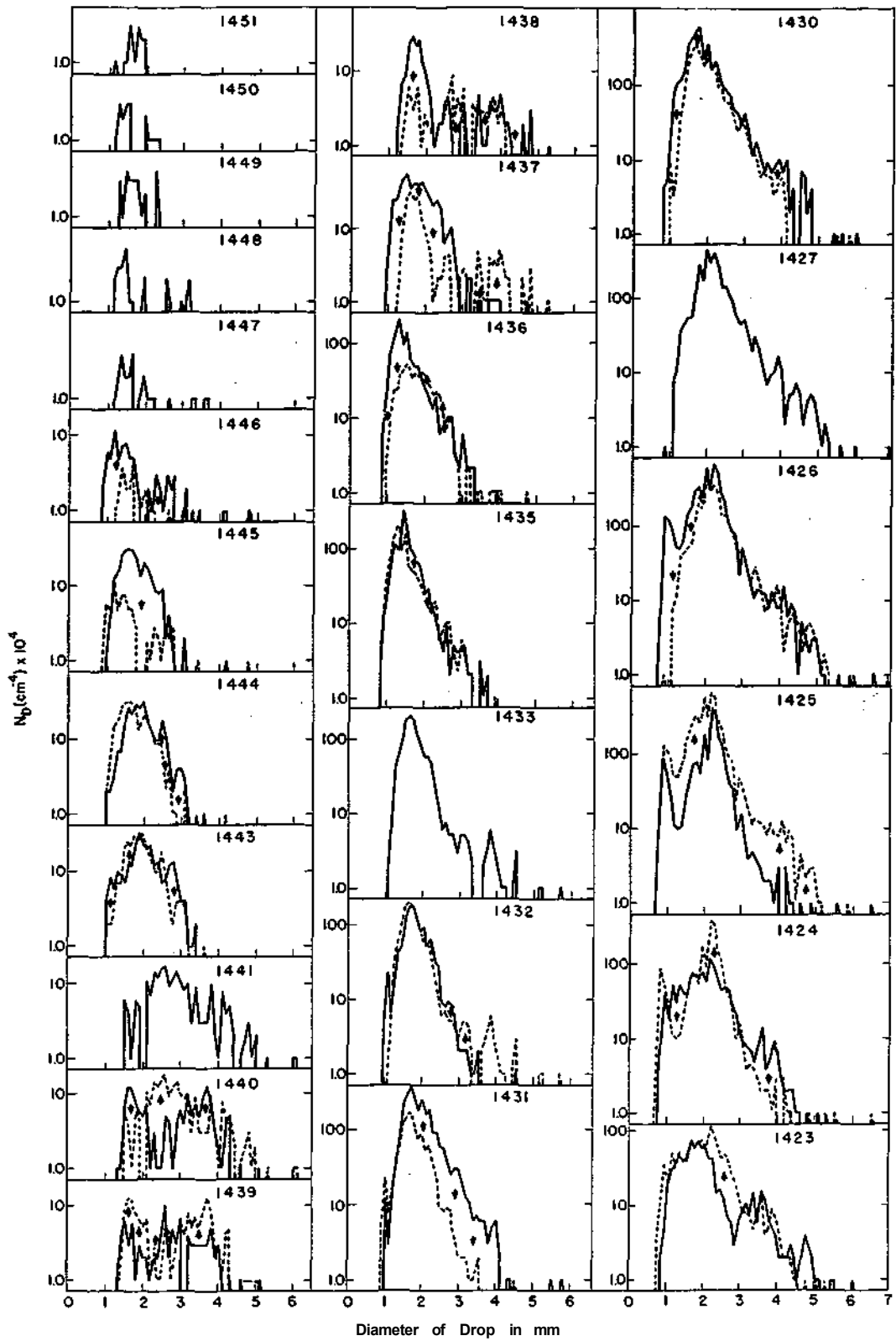
FIG.9a EXAMPLES OF CHRONOLOGICAL SERIES OF N_D CURVES. 1423-1451 EST 5/13/58
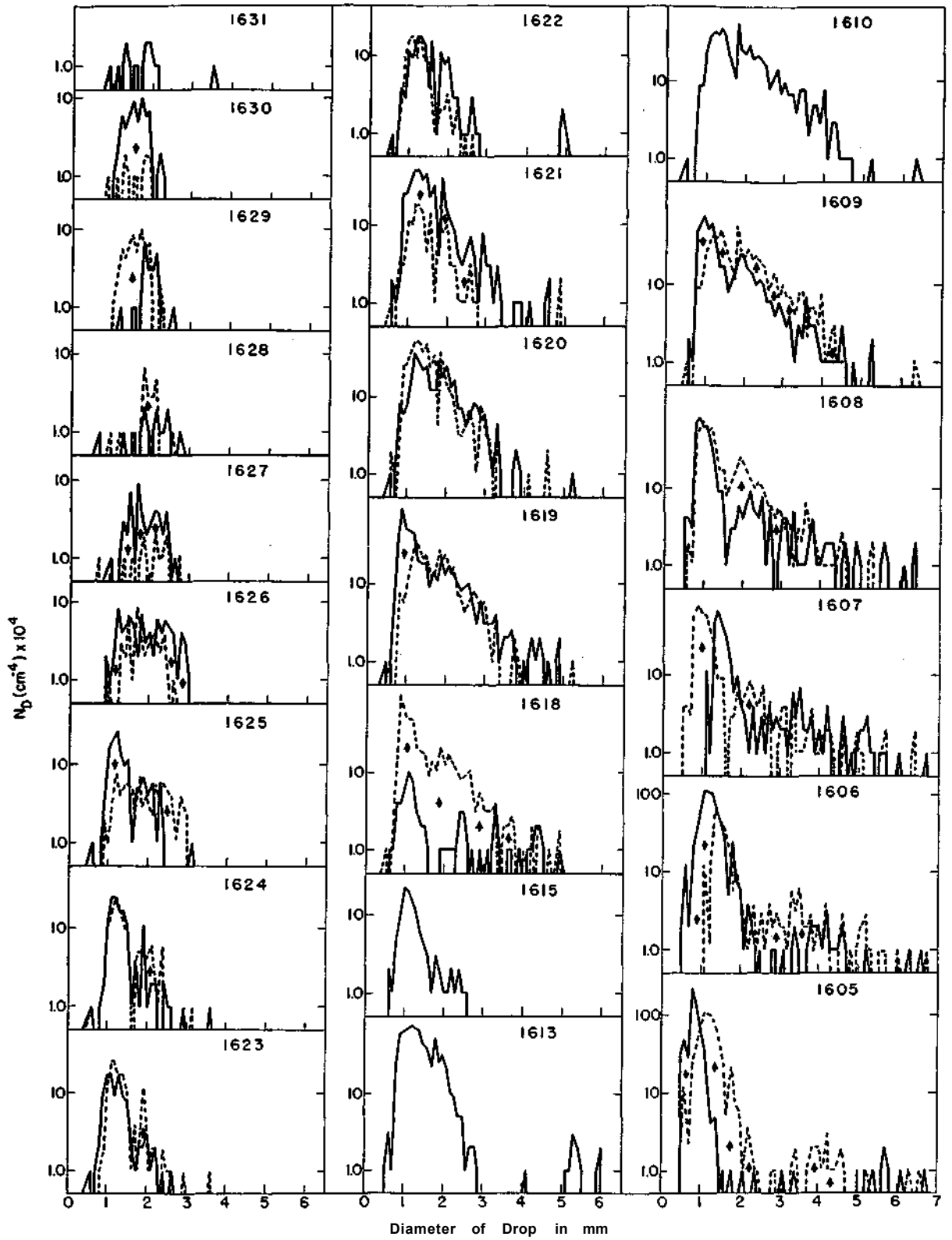
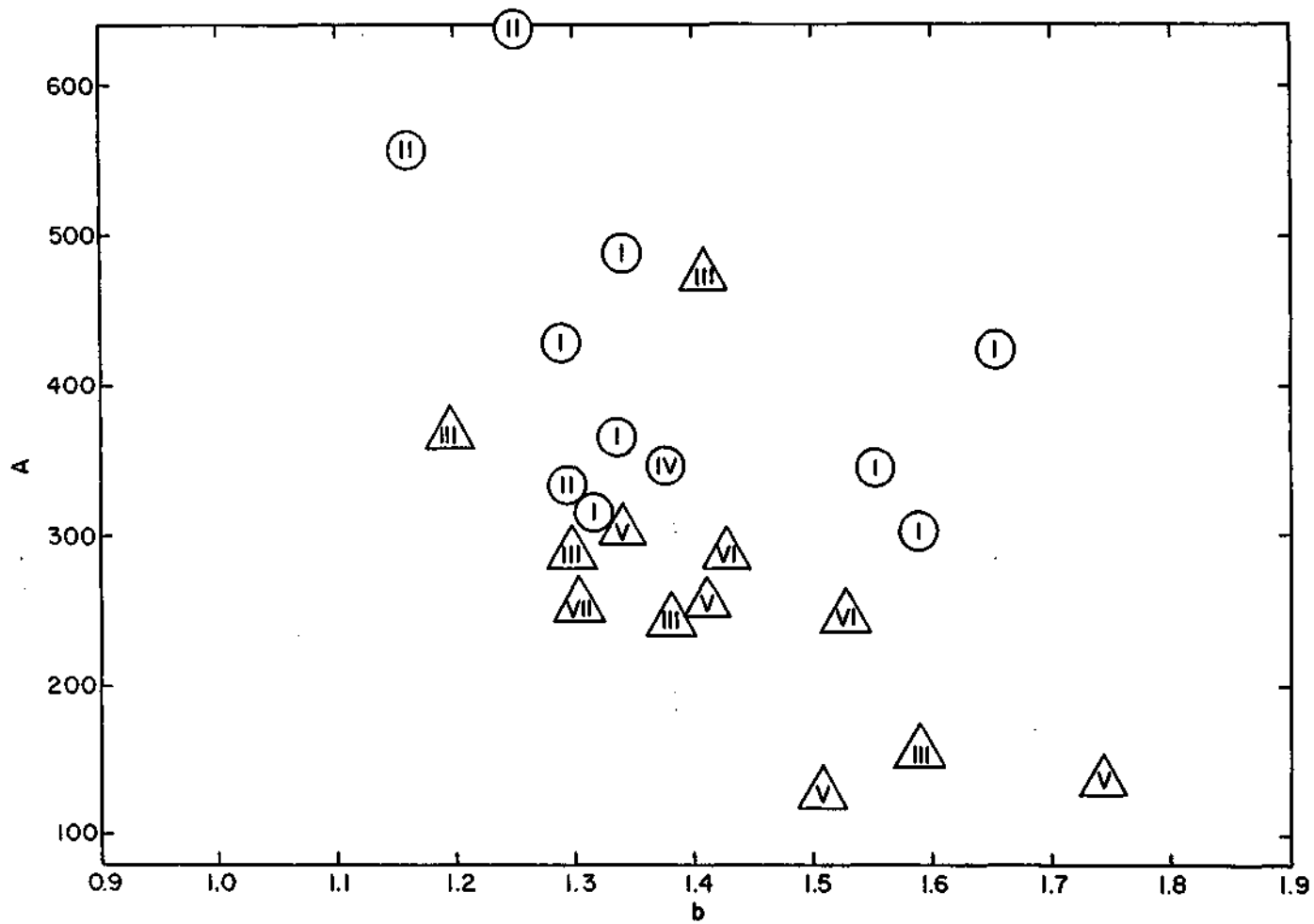FIG.9b EXAMPLES OF CHRONOLOGICAL SERIES OF N$_D$ CURVES, 1605-1631 EST 7/25/58

FIG. 10 RELATIONSHIP BETWEEN PARAMETERS A AND b IN CONVECTIVE STORMS AND TYPES OF RAINGAGE TRACES. (SEE FIG.5 FOR RAIN-GAGE TRACES.)
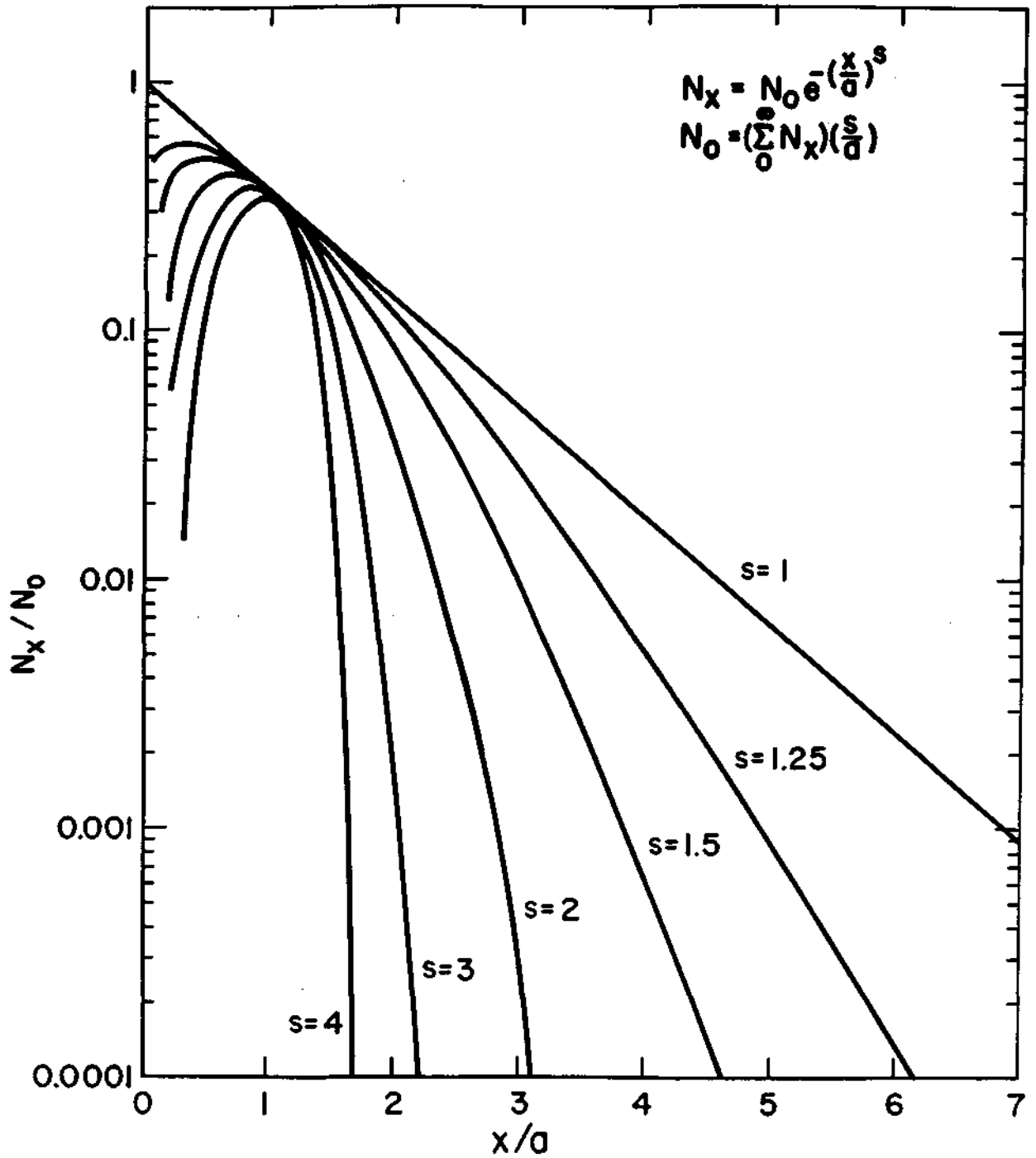
$$N_X = N_O \, \bar{e}^{\left(\frac{x}{a}\right)^s}$$

$$N_O = \left(\sum_0^\infty N_X\right)\left(\frac{s}{a}\right)$$

s= 1

s= 1.25

s= 1.5

s= 2

s= 3

s= 4

N_X / N_O

x/a

FIG.II ILLUSTRATION OF CURVES GIVEN BY EQUATION 6.
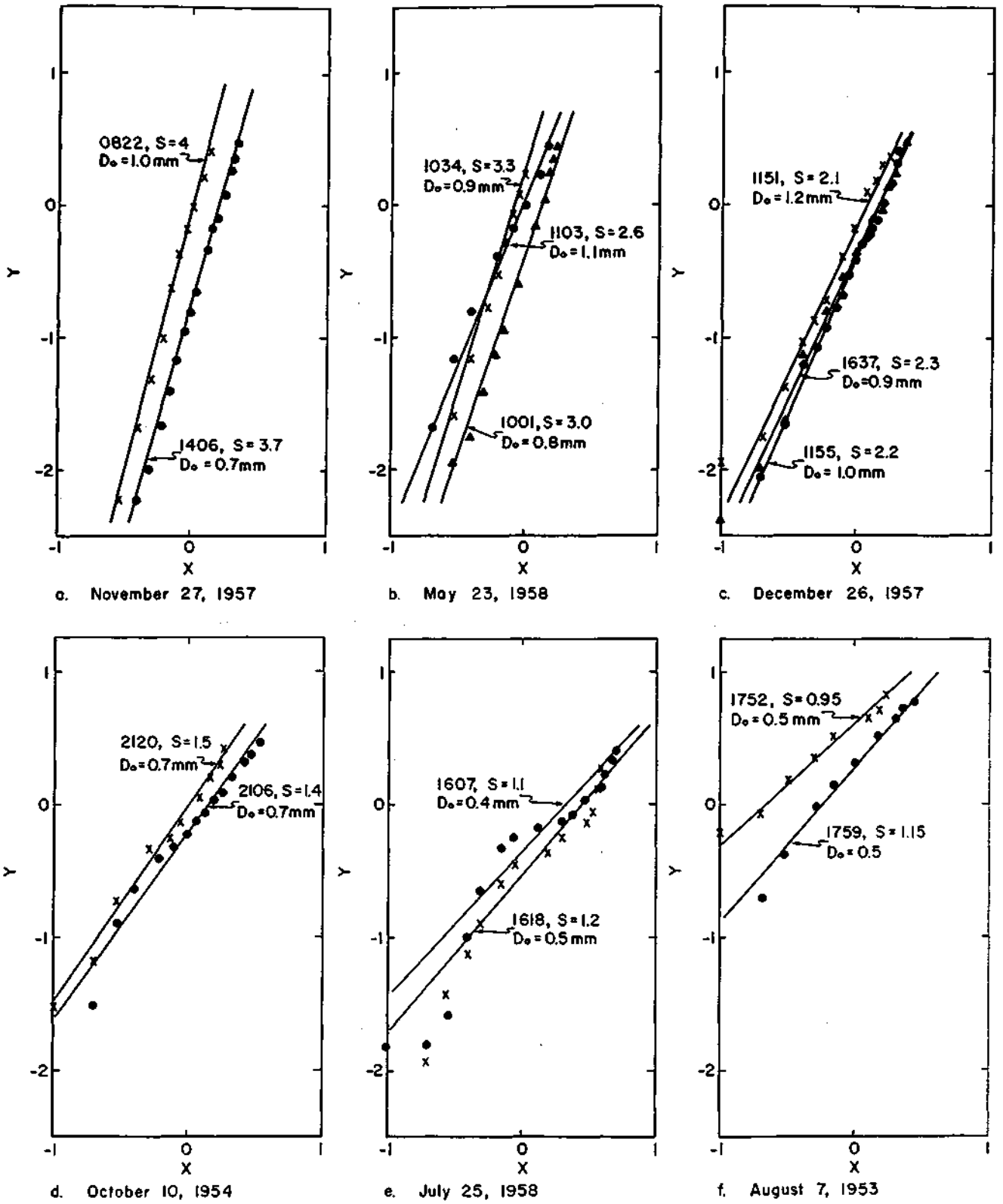
FIG. 12   FITTING   EQUATION   6   TO N_D DATA   SELECTED   FROM   FIG. 8
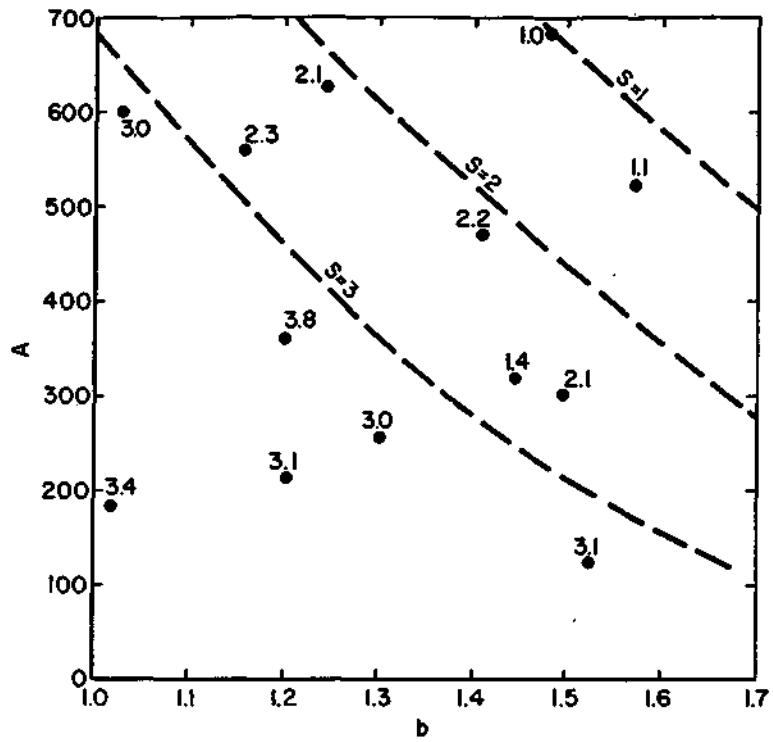
FIG. 13   THE RELATION OF THE SKEWNESS PARA-
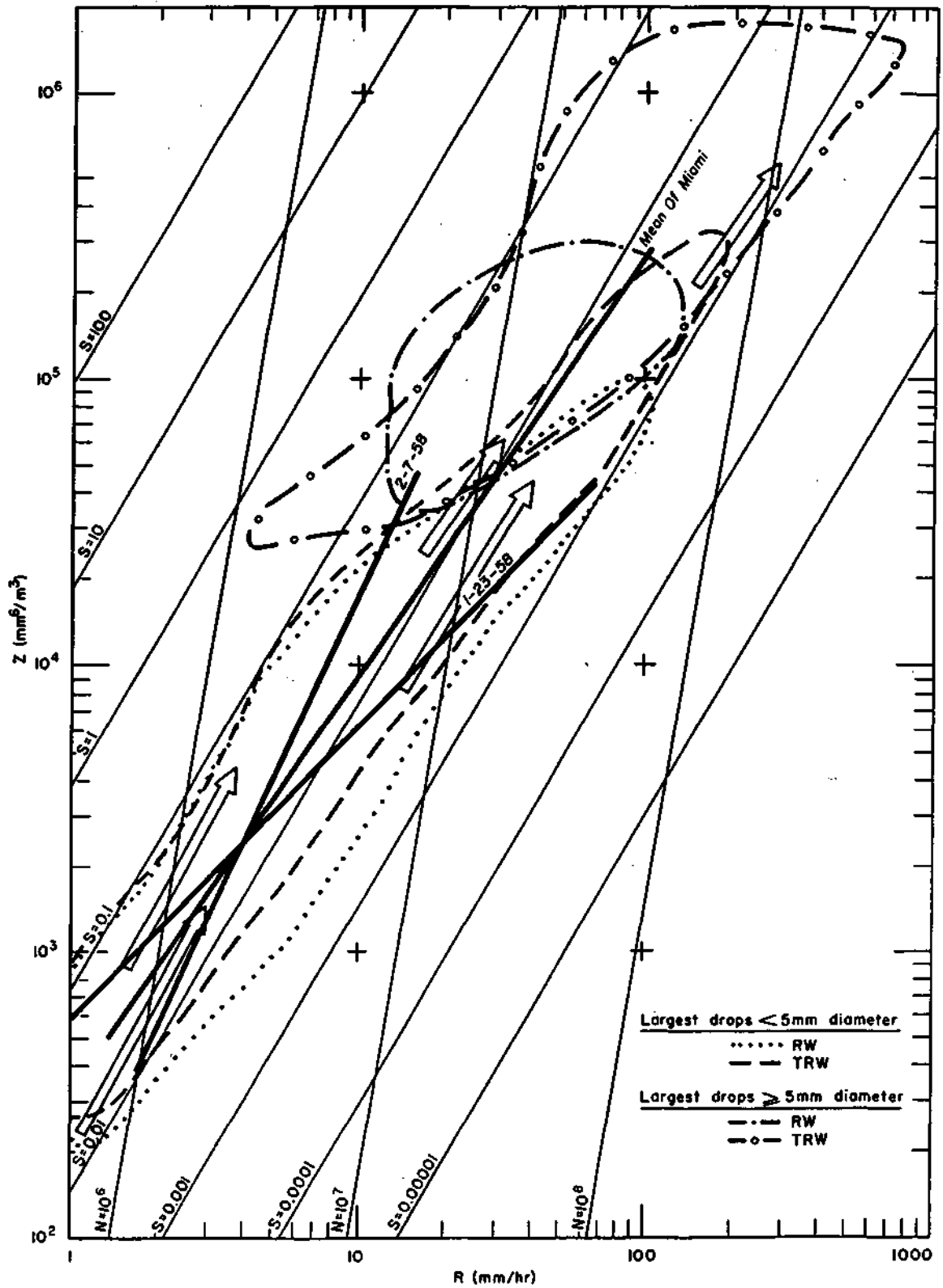METER (s) OF ND CURVES ON A, b CO-
ORDINATES.

FIG.14   Z R-RELATION FOR RANDOM COALESCENCE PROCESS

FIG. 15   PLOT OF (A) AGAINST SURFACE MIXING RATIO